

4

Drift and diffusion of charges in gases

4.1 Generalities

Ions and electrons released in a gas by ionizing encounters swiftly lose their energy in multiple collisions with surrounding molecules and acquire the thermal energy distribution of the medium. Under the action of moderate external electric fields, charges move through the medium while diffusing, until neutralized either by recombination in the gas or at the walls. For ions, a process of charge transfer is possible with a molecule of its own gas or of another species having lower ionization potential. Electrons, wandering in the gas and colliding with the molecules, can be neutralized by a positive ion, attach to a molecule having electron affinity, or get absorbed at the walls of the containment vessel.

Most quantities to be discussed here (mobility, drift velocity, diffusion, ...) depend on the gas density, a function itself of temperature, and are therefore inversely proportional to pressure. The appropriate invariant for the field-dependent variables is the ratio E/P , expressed in classic works in units of V/torr, or E/N where N is the Loschmidt constant (number of molecules per unit volume). In modern detector practice it is customary, however, to present data as a function of field at normal temperature and pressure (NTP: 20 °C, one atmosphere). For different conditions, appropriate density-dependent scaling rules should be used (see Section 3.2).

4.2 Experimental methods

The drift and diffusion of charges under the effect of electric and magnetic fields has been a classic subject of research for decades in the field named gaseous electronics. Major outcomes of these studies are a detailed knowledge of molecular collision processes and of the electron–molecule cross sections; methods and results are discussed in numerous textbooks (Loeb, 1961; Brown, 1959; Hasted, 1964; Massey *et al.*, 1969; Huxley and Crompton, 1974).

Drift properties of ions and electrons are studied with devices named drift tubes, which have designs that can vary from the very sophisticated systems used for fundamental gaseous electronics studies to the simpler structures introduced in the development of modern gaseous detectors (see Section 4.7). For ions, due to many possible processes of charge transfer and chemical reactions between excited species, and the consequent sensitivity to very small amounts of pollutants, the systems used for fundamental studies are built with clean materials and are thoroughly outgassed using vacuum technologies. A detailed description of drift tubes and experimental methods can be found for example in McDaniel and Mason (1973).

In its basic design, a drift tube generates charges (ions or electrons) at a known time at one end of a region with a uniform electric field, and permits one to measure the distribution of arrival time of the charges at a collecting electrode, wire or plate, after the drift; the measurement can be done in a current mode, or with detection of the individual pulses. For ions, the source is usually an electron-impact ion beam, admitted through a control grid to the main section of the tube by microsecond-wide gating pulses, much shorter than the total drift time to be measured, which is typically from several hundred microseconds to milliseconds. The distance between source and detector can be varied; in some systems, the ion beam enters the tube through several ports, at different distances from the collecting anode. The tube's end can be coupled to a mass spectrometer, permitting a positive identification of the ion species. Figure 4.1 is a schematic cross section of

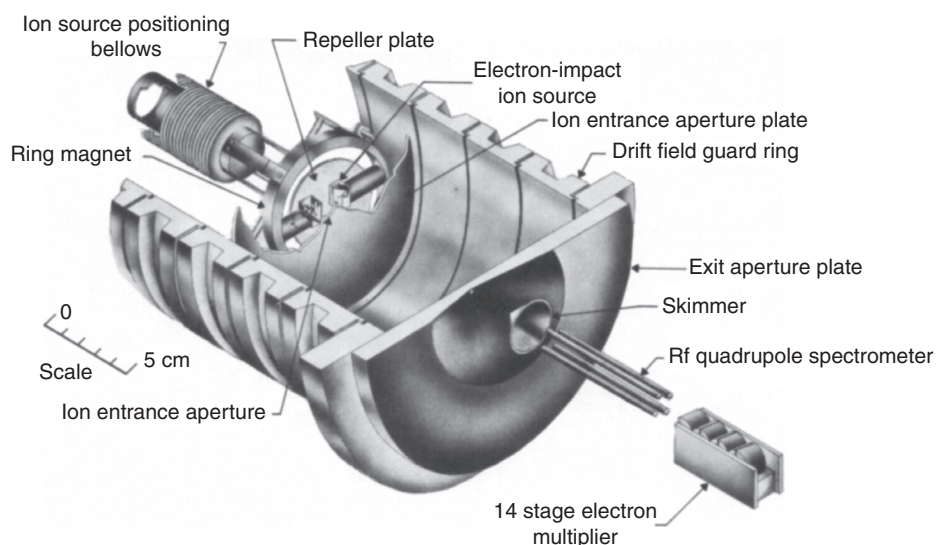


Figure 4.1 A drift tube with ion source, drift volume and mass spectrometer for ion identification (Thomson *et al.*, 1973). By kind permission of The American Institute of Physics.

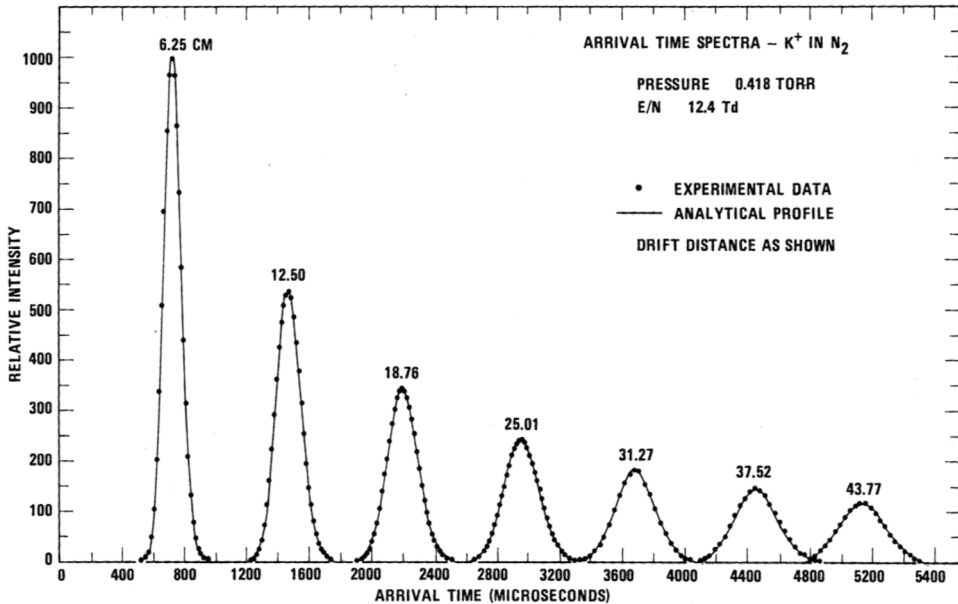


Figure 4.2 Spectra of arrival time of ions in a drift tube for several source positions (Thomson *et al.*, 1973). By kind permission of The American Institute of Physics.

one such devices, showing the movable ion source, the drift volume and the end detector spectrometer for ion sampling (Thomson *et al.*, 1973); Figure 4.2, from data by the same authors, gives an example of ion current recorded in the drift tube as a function of time for seven position of a K^+ ions source in nitrogen (McDaniel and Mason, 1973). A fit to the peak of the distributions provides the average drift time per unit length of migration (the drift velocity), and the width the longitudinal diffusion, in the direction of drift, after correcting for the width of the original beam.

Simpler methods to measure the ions drift properties have been used in the course of modern detectors development, restricting the study to the species produced in the gas by the electron–molecule collisions during avalanche multiplication. In its basic conception, the instrument is a drift chamber structure exposed to an ionizing source; the anodic signal, produced by the electron avalanche on the wire, provides the time reference, and the ions' drift time is recorded detecting their arrival on a cathode wire or a collection plate, screened by a grid, at the end of the drift region (see for example Schultz *et al.*, 1977). While not providing a positive identification of ions, the slopes of the mobility curves, measured while varying the gas composition, suggest the type of dominant ion (see Section 4.4).

Drift tubes used for the measurement of electron drift properties are similar in design, but require a time reference that can be obtained with short electron bursts

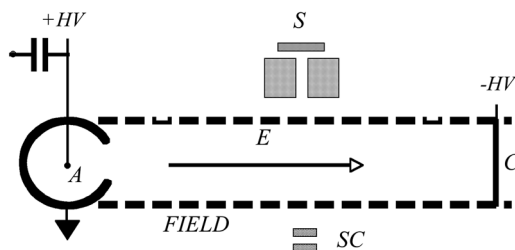


Figure 4.3 Schematics of a drift chamber. Electrons produced by a collimated charged particle source S drift to the anode A where they are detected after avalanche multiplication. Field electrodes at suitable potentials create a uniform electric field; a pair of scintillation counters SC in coincidence provides the time reference.

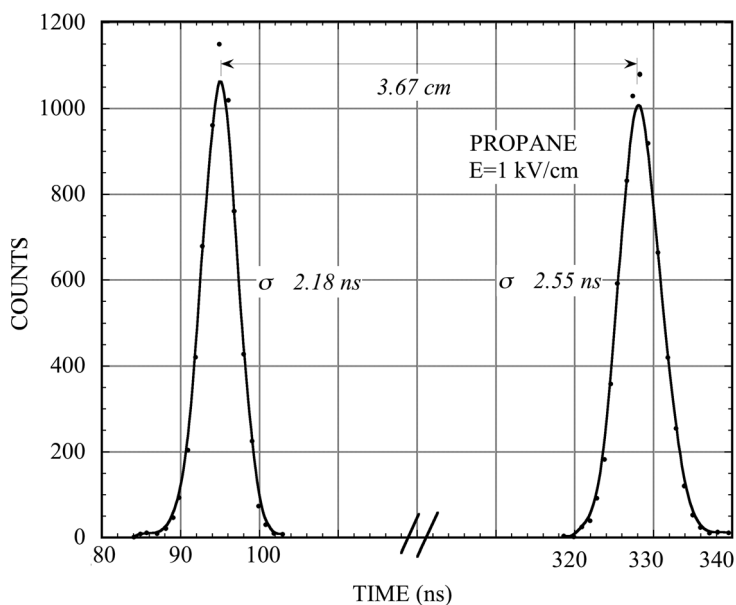


Figure 4.4 Example of electron drift time spectra for two positions of a collimated source (Jean-Marie *et al.*, 1979). By kind permission of Elsevier.

controlled by electrical shutters, or generated by a UV or laser pulse hitting an internal electrode (Huxley and Crompton, 1974; Christophorou *et al.*, 1966). In more recent setups making use of a collimated charged particle beam or radioactive electron sources, the time reference is given by an external set of scintillator counters in coincidence, as shown schematically in Figure 4.3.

Figure 4.4 is an example of arrival time spectra for electrons released by a collimated source at two distances from the anode (Jean-Marie *et al.*, 1979); the time difference between the peaks provides the drift velocity, while the width of

the distribution is a convolution between the longitudinal diffusion of the drifting electrons and the source width (1 mm in this example).

It should be noted that the described devices record only the longitudinal diffusion of charges, in the drift direction; while for ions the diffusion is symmetric, this is not the case for electrons, as discussed in the next sections. The transverse diffusion can be measured using segmented collection electrodes sharing the charge, a method described by Townsend (1947) and used extensively, for example in the development of time projection and micro-pattern chambers (Chapters 10 and 13).

Drift properties in a magnetic field are measured by inserting the detectors into a magnet, if needed adjusting the voltage applied to the field shaping electrodes to compensate for the Lorentz angle; an example is described in Breskin *et al.* (1974b).

4.3 Thermal diffusion of ions

In the absence of external fields and inelastic collision processes, ions and electrons released in a gas behave like neutral molecules, with properties described by the classic kinetic theory of gases. The theory provides the probability of an atom or molecule having an energy ε at the absolute temperature T (Maxwell–Boltzmann law):

$$F(\varepsilon) = 2\sqrt{\frac{\varepsilon}{\pi(kT)^3}} e^{-\frac{\varepsilon}{kT}}, \quad (4.1)$$

where k , Boltzmann's constant, equals 1.38×10^{-16} erg/°K or $8.617 \cdot 10^{-5}$ eV/°K; the distribution does not depend on the mass of the particles. The average thermal energy is obtained by integration over the distribution:

$$\bar{\varepsilon}_T = kT$$

at normal conditions, $\bar{\varepsilon}_T = 0.025$ eV (Figure 4.5).

The corresponding distribution of velocity v for a particle of mass m is:

$$f(v) = 4\pi\left(\frac{m}{2\pi kT}\right)^{\frac{3}{2}} v^2 e^{-\frac{mv^2}{2kT}}, \quad (4.2)$$

by integration, one gets the average value of the velocity:

$$\bar{v} = \int_0^{\infty} v f(v) dv = \sqrt{\frac{8kT}{\pi m}}; \quad (4.3)$$

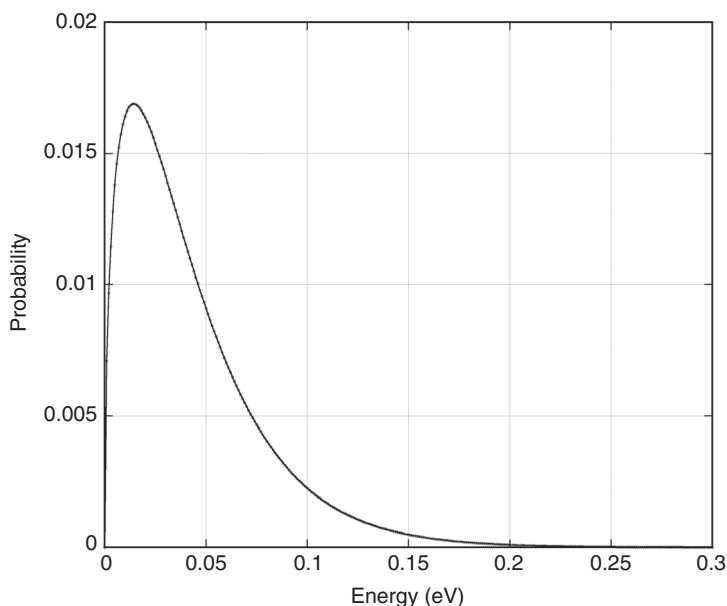


Figure 4.5 Energy distribution of molecules at normal conditions.

the most probable value v_{MP} is:

$$v_{MP} = \sqrt{\frac{2kT}{m}}. \quad (4.4)$$

Figure 4.6 is the computed distribution of the velocity probability for atoms of noble gases at NTP; one can see that they are largely supersonic.

A localized distribution of molecules or ions diffuses symmetrically by multiple collisions following a Gaussian law:

$$\frac{dN}{N} = \frac{1}{\sqrt{4\pi Dt}} e^{-\frac{x^2}{4Dt}} dx, \quad (4.5)$$

where dN/N is the fraction of particles found in the element dx at a distance x from the origin and after a time t ; D denotes a diffusion coefficient. The root mean square of the distribution, or standard deviation, is given for linear and volume diffusion, respectively, by:

$$\sigma_x = \sqrt{2Dt} \text{ and } \sigma_v = \sqrt{6Dt}. \quad (4.6)$$

Classic values of the diffusion coefficient D , mean free path between collisions λ and average velocity v of atoms and molecules in their own gas are given in Table 4.1 (Loeb, 1961).

Expression (4.5) can be used to estimate the time-dependent dilution in a gas volume of a given species, for example ions released in a given position or

Table 4.1 Classic values of the mean free path between collisions, velocity and diffusion coefficient for atoms and molecules at NTP (Loeb, 1961).

Gas	$\lambda(\text{cm})$	$v(\text{cm/s})$	$D(\text{cm}^2/\text{s})$
H ₂	1.8×10^{-5}	2×10^5	0.34
He	2.8×10^{-5}	1.4×10^5	0.26
Ar	1.0×10^{-5}	4.4×10^4	0.04
O ₂	1.0×10^{-5}	5.0×10^4	0.06
H ₂ O	1.0×10^{-5}	7.1×10^4	0.02

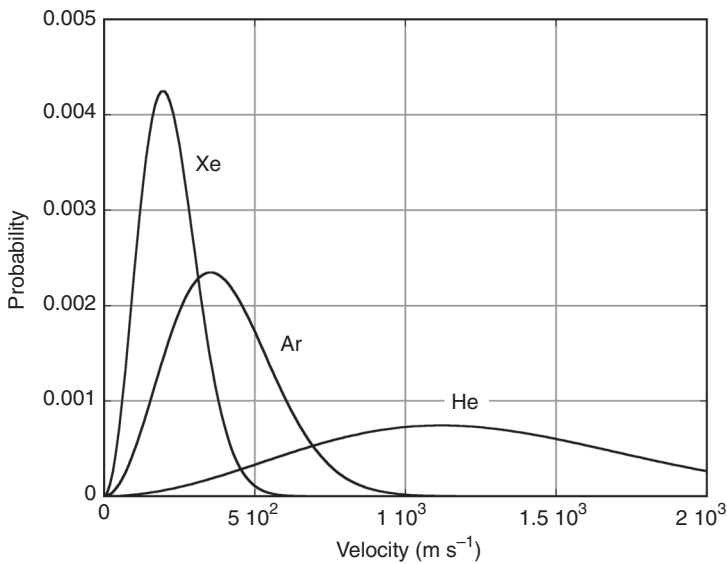


Figure 4.6 Velocity distribution for molecules of different masses (NTP).

pollutants penetrating from a hole in a counter. Figure 4.7 is an example of space distributions of oxygen ions in air, at normal conditions, after different time intervals, computed from the previous expression; after a few seconds, the thermal diffusion spreads a foreign species through the whole counter volume. This implies also that the detector volume can be easily contaminated by a leak; even a small overpressure, resulting in a gas outflow, can hardly compete with the penetration of the very fast foreign molecules into the volume.

4.4 Ion mobility and diffusion in an electric field

When an electric field is applied to the gas volume, a net movement of ions along the field direction is observed. The average velocity of this slow motion (not to be confused with the instant ion velocity v) is named the drift velocity w^+ , and is

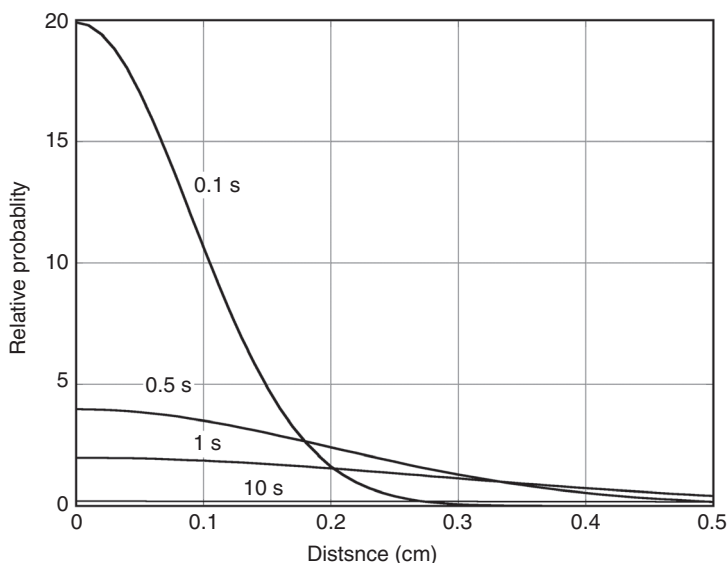


Figure 4.7 Space distribution of initially localized oxygen molecules after increasing time intervals (NTP).

linearly proportional to the electric field up to very high values of E , Figure 4.8 (McDaniel and Mason, 1973). It is therefore customary to define a quantity μ , the ion mobility, as:

$$\mu = \frac{w^+}{E}. \quad (4.7)$$

The value of the mobility is specific to each ion moving in a given gas, and depends on pressure and temperature through the expression:

$$\mu(P, T) = \frac{T P_0}{T_0 P} \mu(P_0, T_0). \quad (4.8)$$

A constant mobility is the direct consequence of the fact that, up to very high fields, the average energy of ions is almost unmodified; as will be seen later, this is not the case for the electrons.

A classic argument allows one to obtain the following relationship between mobility and diffusion coefficient (Nernst–Townsend formula¹):

$$\frac{D}{\mu} = \frac{kT}{e}, \quad (4.9)$$

where D is the diffusion coefficient, and e the electron charge.

¹ Often improperly named the Einstein formula, from his later works on Brownian motion.

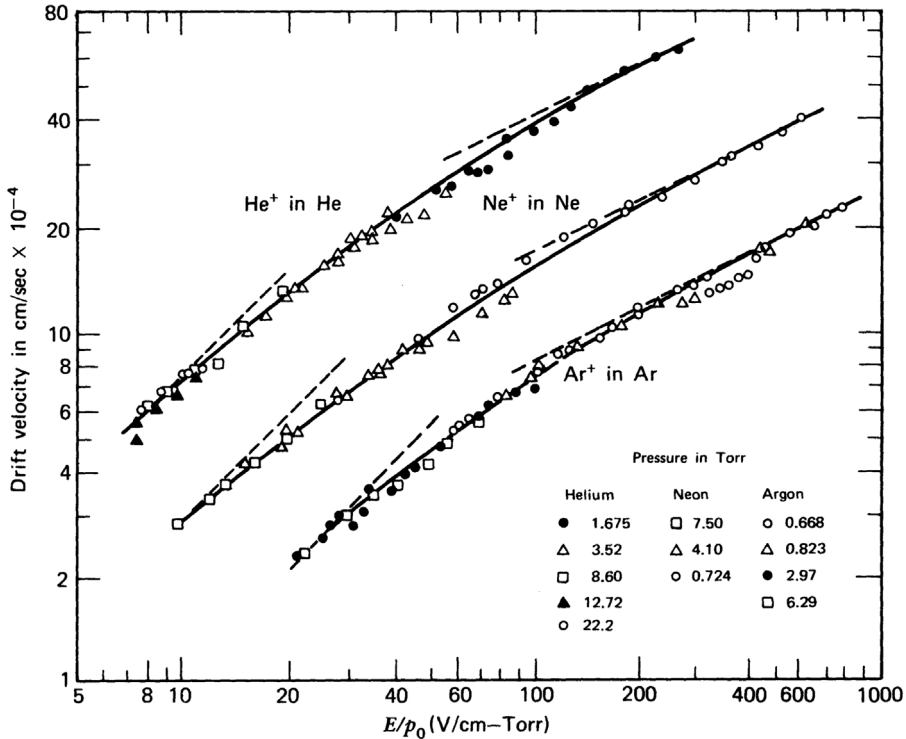


Figure 4.8 Drift velocity of several ions in their own gas as a function of field (McDaniel and Mason, 1973). Reproduced with kind permission of John Wiley & Sons, Inc.

Ions migrating for a time t over a length x diffuse with a probability distribution given by (4.5) and with a linear standard deviation along the drift direction obtained by combining the previous expressions:

$$\sigma_x = \sqrt{\frac{2kT}{e} \frac{x}{E}}; \tag{4.10}$$

the space diffusion therefore does not depend on the type of ion and pressure, but only on the field (Figure 4.9).

The mobility of an ion in a different gas follows in good approximation a simple dependence on the mass ratio (Langevin's law):

$$\mu_I = \sqrt{\left(1 + \frac{M_M}{M_I}\right)}, \tag{4.11}$$

where M_M and M_I are the molecular weights of the support gas and of the migrating ions.

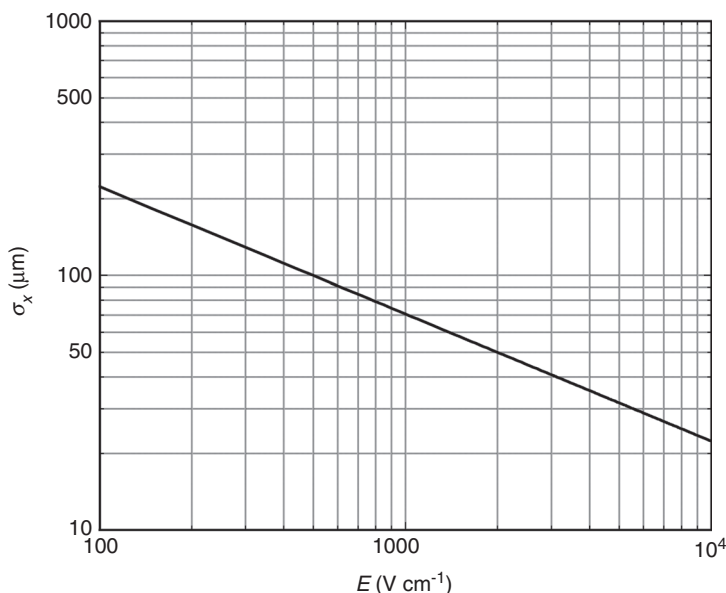


Figure 4.9 RMS of diffusion of ions in the drift direction as a function of field (NTP).

Figure 4.10 is a classic measurement of the mobility of nitrogen ions in various gases, and illustrates the inverse square root dependence on mass (Mitchell and Ridler, 1934). A notable exception is the mobility of the N_2 ion itself, due to a process of charge transfer between the ion and its molecule, energetically possible for ions in their own gas (all other molecules in the plot have ionization potentials larger than that of nitrogen).

In a mixture of gases G_1, G_2, \dots, G_N the mobility μ_i of the ion G_i^+ is given by the relation (Blanc's law):

$$\frac{1}{\mu_i} = \sum_{j=1}^n \frac{p_j}{\mu_{ij}}, \quad (4.12)$$

where p_j is the volume concentration of gas j in the mixture, and μ_{ij} the mobility of ion G_i^+ in the gas G_j .

In gas mixtures, a very effective process of collisional charge transfer can take place, quickly removing all ions except those with the lowest ionization potential. Depending on the nature of the ions and on the difference in ionization potentials (small differences increase the charge transfer probability), it takes between 100 and 1000 collisions for an ion to transfer its charge to a molecule having a lower potential. Since the mean free path for collisions under normal conditions is around 10^{-5} cm (see Table 4.1), after a drift length between $10^{-3}/p$ and $10^{-2}/p$ centimetres,

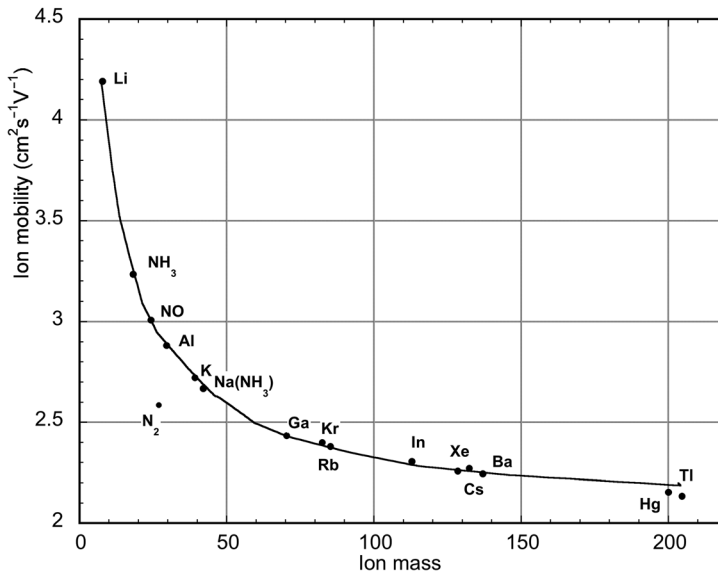


Figure 4.10 Mobility of N₂ ions in different gases (Mitchell and Ridler, 1934).

where p is the percentage of the molecules with lowest ionization potential, the charge transfer mechanism will have left only one species of ions migrating.

Experimental values of mobility for ions in various gases, including their own, are given at normal conditions in Table 4.2, from various sources. In most cases, the exact nature of the drifting ions has not been identified directly; therefore, the values indicated might correspond to an average over several species. With the exception of light ions, most values are rather similar; as will be discussed later, this has the practical consequence that the ions' clearing time in detectors is almost independent of the gas used.

Figure 4.11 and Figure 4.12 provide examples of the measured dependence of the inverse mobility of ions in binary mixtures of Ar-CO₂ (Schultz *et al.*, 1977), Ar-C₃H₈ and CF₄-C₃H₈ (Yamashita *et al.*, 1992) as a function of the gas density or fraction of the molecular component; the values follow Blanc's law well, under the assumption that the drifting ion is the molecule with the lowest ionization potential.

As can be inferred from expression (4.12), for a given ion drifting in a mixture, the inverse mobility depends linearly on the mixture's specific weight; lines of equal slope therefore represent the migration of the same kind of ion. Figure 4.13 shows experimental values of ion mobility in mixtures of argon-isobutane and argon-isobutane-methylal as a function of their density (Schultz *et al.*, 1977).

Although the ion species were not identified in this measurement, the converging slopes of the curves can be interpreted as curve F providing the mobility of

Table 4.2 Mobility of ions, from various sources. Data without a reference are average values from compilations in McDaniel and Mason, 1973).

Gas	Ion	μ (cm ² V ⁻¹ s ⁻¹)
H ₂	Self	13.0
He	Self	10.2
Ar	Self	1.7
Ar	CH ₄	1.87 (Schultz <i>et al.</i> , 1977); 2.07 (Yamashita <i>et al.</i> , 1992)
Ar	C ₂ H ₆	2.06 (Yamashita <i>et al.</i> , 1992)
Ar	C ₃ H ₈	2.08 (Yamashita <i>et al.</i> , 1992)
Ar	i-C ₄ H ₁₀	1.56 (Schultz <i>et al.</i> , 1977); 2.15 (Yamashita <i>et al.</i> , 1992)
Ar	CO ₂	1.72
Ar	(OCH ₃) ₂ CH ₂	1.51
CH ₄	Self	2.22 (Yamashita <i>et al.</i> , 1992)
C ₂ H ₆	Self	1.23 (Yamashita <i>et al.</i> , 1992)
C ₃ H ₈	Self	0.793 (Yamashita <i>et al.</i> , 1992)
i-C ₄ H ₁₀	Self	0.612 (Yamashita <i>et al.</i> , 1992)
i-C ₄ H ₁₀	(OCH ₃) ₂ CH ₂	0.55 (Schultz <i>et al.</i> , 1977)
(OCH ₃) ₂ CH ₂ (Methylal)	Self	0.26 (Schultz <i>et al.</i> , 1977)
O ₂	Self	2.2
CO ₂	Self	1.09
H ₂ O	Self	0.7
CF ₄	Self	0.96 (Yamashita <i>et al.</i> , 1992)
CF ₄	CH ₄	1.06 (Yamashita <i>et al.</i> , 1992)
CF ₄	C ₂ H ₆	1.04 (Yamashita <i>et al.</i> , 1992)
CF ₄	C ₃ H ₈	1.04 (Yamashita <i>et al.</i> , 1992)

isobutane ions in argon–isobutane mixtures, curve A the mobility of methylal in argon–methylal and curves B, C, D, E the mobility of methylal ions in argon–isobutane–methylal mixtures. In the range of electric fields considered (a few hundred to a thousand V/cm) and for 1 cm of drift, if more than 3–4% methylal is added to the mixture, the exchange mechanism is fully efficient and the measurement is consistent with the assumption that only those ions are left migrating. The process is exploited in gaseous detectors to effectively remove organic ions produced in the avalanches, having the tendency to form polymers, transferring the charge to a non-polymerizing species, such as alcohols, methylal and others (see Chapter 16).

4.5 Classic theory of electron drift and diffusion

Electrons released in a gas by ionization quickly reach thermal equilibrium with the surrounding molecules; in the absence of external fields, their energy

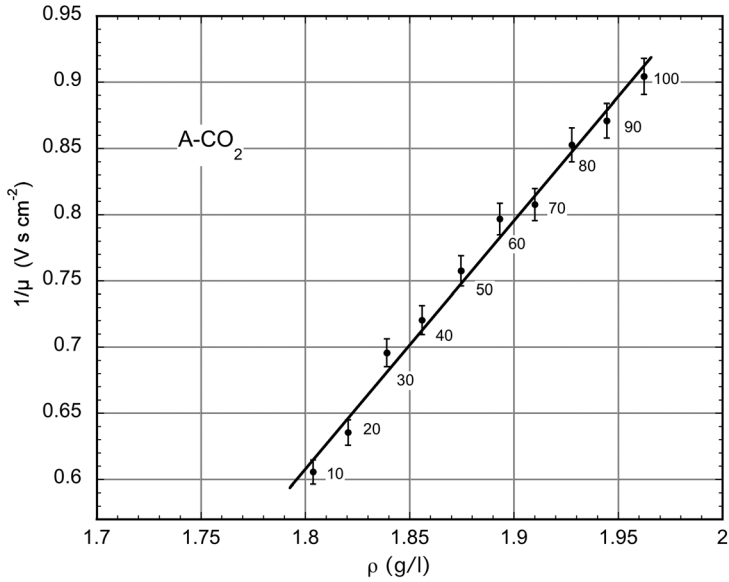


Figure 4.11 Inverse mobility of CO₂ ions in argon-CO₂ as a function of density of the mixture (Schultz *et al.*, 1977). By kind permission of EDP Science Journals.

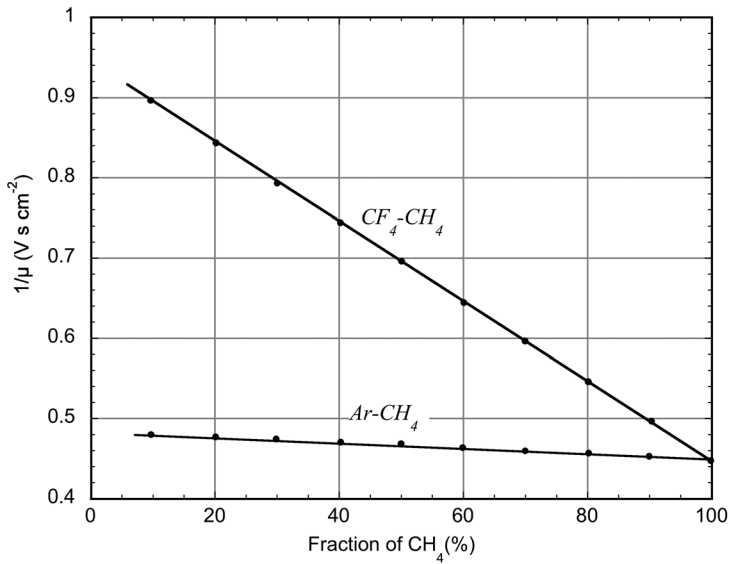


Figure 4.12 Inverse ion mobility in argon-methane and carbon tetrafluoride-methane mixtures (Yamashita *et al.*, 1992). By kind permission of Elsevier.

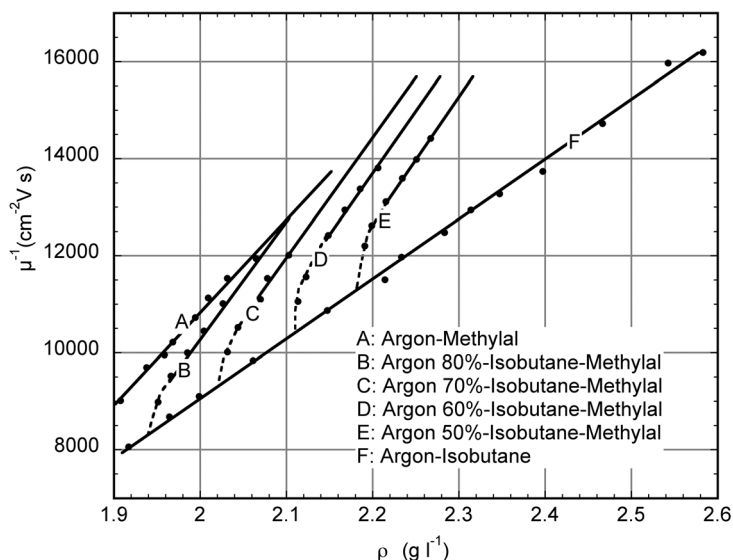


Figure 4.13 Inverse mobility in argon–isobutane–methylal mixtures, as a function of density (Schultz *et al.*, 1977). By kind permission of EDP Science Journals.

distribution follows the same law as for ions, see expression (4.1). However, due to the lower mass, their thermal velocity is several orders of magnitude higher, as one can deduce from (4.3), with an average value at room temperature of about 10^7 cm/s. Thermal diffusion occurs with a correspondingly larger value of the diffusion coefficient.

Free electrons can be neutralized by an ion, absorbed in the walls, or attach to a molecule having electron affinity or being electro-negative; the probability of attachment per collision, h , negligible for noble gases, has finite values for gases having incomplete outer electronic shells, as can be seen in Table 4.3 (Fulbright, 1958; Loeb, 1961; Townsend, 1947). The table also shows the average attachment time $t_h = 1/hN$, where N is the number of collisions per unit time. In oxygen, for example, the average time needed for a thermal electron to be attached is about 200 ns.

Adding a percentage p of an electro-negative molecule to a main gas mixture, the probability of attachment is hp . As discussed later, the attachment coefficient is a strong function of the electron energy, hence of the field.

When an electric field is present, the electron swarm moves in the direction opposite to the field vector; a simple theory of mobility can be formulated along the same lines as for positive ions. It was found very early, however, that except for very low fields, the mobility of electrons is not constant: because of their small mass, electrons can substantially increase their energy between collisions with the

Table 4.3 *Electron attachment probability, frequency of collisions and average attachment time for several gases at NTP.*

Gas	h	$N(\text{s}^{-1})$	$t_h(\text{s})$
CO ₂	6.2×10^{-9}	2.2×10^{11}	0.71×10^{-3}
O ₂	2.5×10^{-5}	2.1×10^{11}	1.9×10^{-7}
H ₂ O	2.5×10^{-5}	2.8×10^{11}	1.4×10^{-7}
Cl	4.8×10^{-4}	4.5×10^{11}	4.7×10^{-9}

gas molecules. In a simple formulation (Townsend, 1947), the electron drift velocity can be written as:

$$w^- = k \frac{eE}{m} \tau, \quad (4.13)$$

where τ is the mean time between collisions. The value of the constant k , between 0.75 and 1, depends on assumptions about the energy distribution of electrons, see for example Palladino and Sadoulet (1974). While convenient for qualitative considerations, Townsend's expression is not very useful in practice, since the values of w^- and τ depend on the gas and field.

During the drift in electric fields, and as a result of multiple collisions with molecules, electrons diffuse, spreading the initially localized charge cloud. The extent of diffusion depends on the gas, but also strongly on E , due to the increase of the electron energy. To take this into account, expression (4.9) can be modified by introducing a phenomenological quantity ε_k , named characteristic energy:

$$\frac{D}{\mu} = \frac{\varepsilon_k}{e}; \quad (4.14)$$

for thermal electrons, $\varepsilon_k = kT$, and the expression reduces to the previous one. The linear space diffusion over the distance x can then be written as:

$$\sigma_x = \sqrt{\frac{2}{e} \frac{\varepsilon_k x}{E}}. \quad (4.15)$$

Expression (4.10) can be rewritten to show explicitly the dependence on the reduced field E/P :

$$\sigma_x = \sqrt{\frac{2\varepsilon_k}{e}} \sqrt{\frac{P}{E}} \sqrt{\frac{x}{P}}. \quad (4.16)$$

4.6 Electron drift in magnetic fields

The presence of an external magnetic field modifies the drift properties of the swarm of electrons. The Lorentz force exerted on moving charges alters the linear

segment of motion between two collisions into circular trajectories, and can affect the energy distribution; the net effect is a reduction of the drift velocity, and a drift of the swarm along a direction at an angle with the electric field lines.

The simple theory provided by expression (4.13) permits computation of the effect on velocity and diffusion for the two particular cases of perpendicular and parallel fields:

$$\vec{E} \perp \vec{B} \quad \tan \theta_B = \omega \tau$$

$$w_B = \frac{E}{B} \frac{\omega \tau}{\sqrt{1 + \omega^2 \tau^2}}, \quad (4.17)$$

$$\vec{E} // \vec{B} : w_B = w_0,$$

$$\sigma_L = \sigma_0,$$

$$\sigma_T = \frac{\sigma_0}{\sqrt{1 + \omega^2 \tau^2}}, \quad (4.18)$$

where θ_B is the angle between the drifting swarm and the electric field in the plane perpendicular to \vec{B} , $\omega = EB/m$ is the Larmor frequency and τ is the mean collision time. For perpendicular fields, the swarm drifts at an angle to the electric field, with a reduced drift velocity; for parallel fields in contrast the magnetic drift velocity and the longitudinal diffusion are unaffected, while the transverse diffusion, perpendicular to the fields, is reduced by a factor that depends on the product $\omega\tau$. This effect is exploited to substantially improve the space resolution in drift and time projection chambers.

In the general case of arbitrary directions of electric and magnetic fields, the so-called friction force theory provides the following expression:

$$\vec{w} = \frac{e}{m} \frac{\tau}{1 + \omega^2 \tau^2} \left[\vec{E} + \omega \tau \frac{\vec{E} \times \vec{B}}{B} + \omega^2 \tau^2 \frac{\vec{B} (\vec{E} \cdot \vec{B})}{B^2} \right]. \quad (4.19)$$

4.7 Electron drift velocity and diffusion: experimental

The experimental measurements of electron drift and diffusion properties, accompanied by the development of electron transport theories, have been a major subject of research from the 1920s through to the 1950s. Due to the extreme sensitivity of the measurements to trace pollutants, particularly in pure noble gases, results were often controversial. Addition to rare gases of controlled amounts of molecular additives, as needed in gaseous counters to guarantee

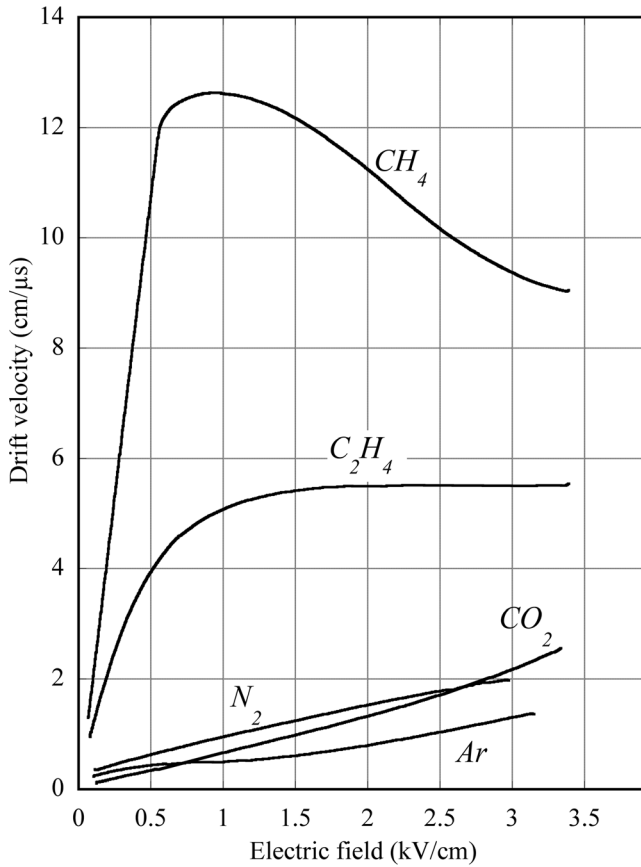


Figure 4.14 Electron drift velocity as a function of field in pure gases at NTP (Sauli, 1977). By kind permission of CERN.

stable and high gain operation, generated abundant phenomenological literature on the subject. Many compilations exist, from classic works (Brown, 1959; Loeb, 1961; Christophorou, 1971) to detector-oriented data collections (Peisert and Sauli, 1984). With the development of dedicated electron transport simulation programs, described in Section 4.10, drift properties of electrons in most gases and mixtures commonly used in detectors can be computed with high accuracy in a wide range of electric fields, including the region of avalanche multiplication. Only selected representative examples of experimental measurements will be presented here.

The compilation in Figure 4.14 for several pure gases illustrates the wide span of values and shape of the field-dependence of the drift velocity (Sauli, 1977). The addition of even very small fractions of one gas to another, which modify the average energy, can dramatically change the drift properties;

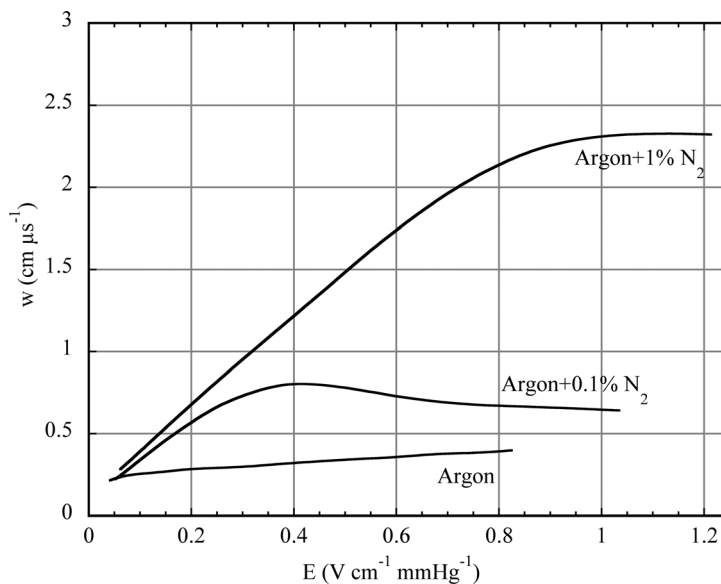


Figure 4.15 Effect on drift velocity of small nitrogen addition (Colli and Facchini, 1952). By kind permission of the American Institute of Physics.

as mentioned, it has a particularly strong effect for noble gases, as illustrated in Figure 4.15 (Colli and Facchini, 1952).

In the course of development of the drift chambers, electrons drift and diffusion properties have been extensively measured as a function of field in many mixtures of noble gases and hydrocarbons. Figure 4.16 is a collection of measurements in argon–isobutane; the curves are the results of early calculations making use of the transport theory, discussed in Section 4.10 (Schultz and Gresser, 1978). The mixture containing around 30% of $i\text{-C}_4\text{H}_{10}$ exhibits a constant, or saturated, drift velocity at moderate values of field, and was therefore selected for the early operation of high-accuracy drift chambers (Breskin *et al.*, 1974b). Figure 4.17 is another example for argon–methane mixtures at NTP (Jean-Marie *et al.*, 1979). The same authors measured the effect on drift velocity of the addition of small quantities of nitrogen, a frequent pollutant in detectors having small leaks (Figure 4.18).

A good knowledge of the dependence of drift velocity on the gas composition and ambient conditions is needed for obtaining stable operation, particularly in high-accuracy drift chambers. This has been for long an experimental issue, until the availability of accurate calculation programs based on the electron transport theory. For ‘cold’ gases, in which the electrons remain thermal up to high field values, the expected relative change in drift velocity is simply related to the change in the gas density and therefore to the absolute temperature, $\Delta w/w = \Delta T/T$.

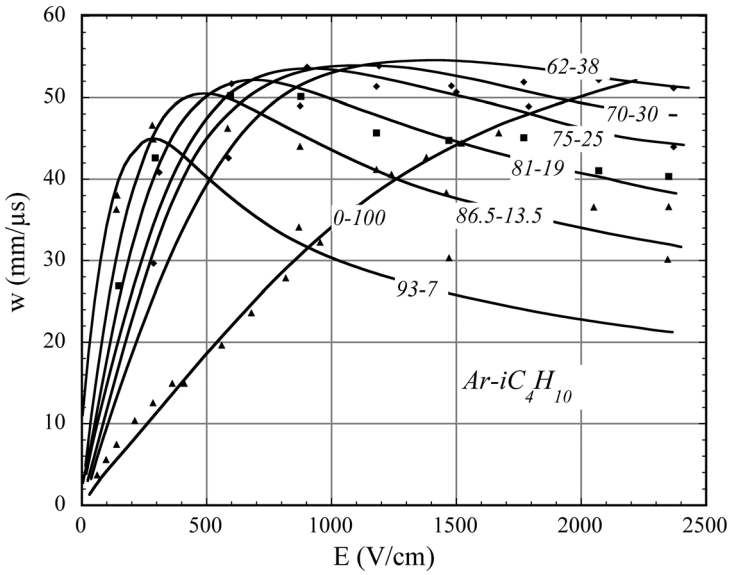


Figure 4.16 Electron drift velocity in argon–isobutane mixtures at NTP (Breskin *et al.*, 1974b). By kind permission of Elsevier.

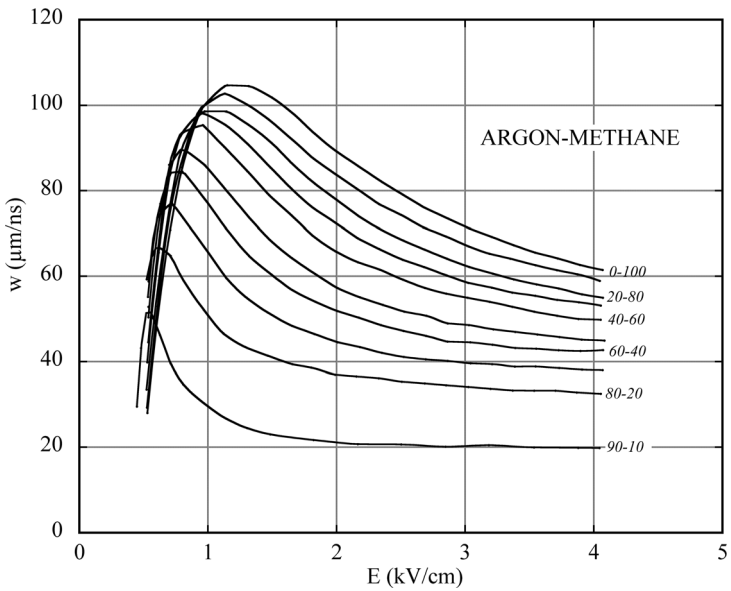


Figure 4.17 Electron drift velocity in argon–methane mixtures at NTP (Jean-Marie *et al.*, 1979). By kind permission of Elsevier.

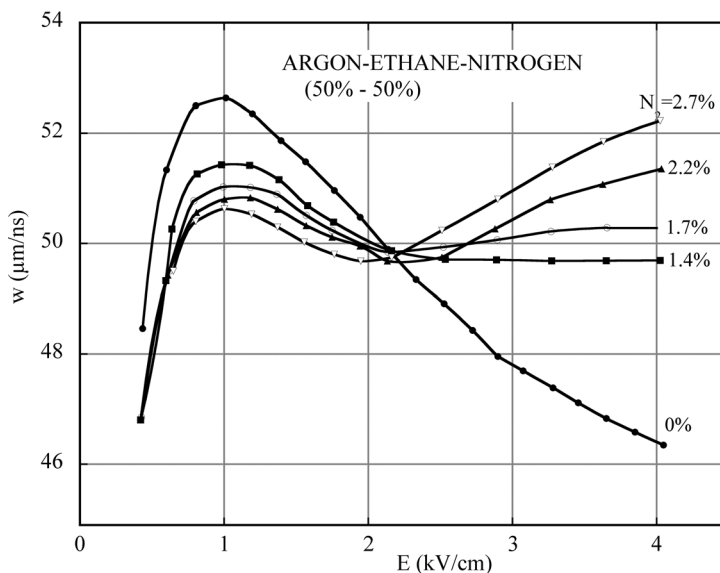


Figure 4.18 Effect on drift velocity of small nitrogen additions to an argon–ethane mixture (Jean-Marie *et al.*, 1979). By kind permission of Elsevier.

When electrons ‘warm up’ under the effect of the electric field, the variation can be larger or smaller, and even negative, depending on the detailed dependence of the electron–molecule cross sections on the electron energy. Figure 4.19 is an example of the estimated relative variation of drift velocity as a function of field for several gas mixtures at NTP per degree of temperature increase; the point with error bars is a measurement (Schultz and Gresser, 1978) and corresponds to the operating conditions selected for the high-accuracy drift chambers (Breskin *et al.*, 1974b). A fundamental parameter for the long-term operation of drift detectors, the temperature dependence of drift velocity has been measured for many other gases; Figure 4.20 is an example of drift time variation as a function of temperature, measured in dimethyl ether (DME) with a time expansion chamber for 34 mm of drift at a field of 164 V/cm, compared with calculations (Hu *et al.*, 2006).

In Figure 4.21 the computed result is shown for a standard argon–methane 90–10 gas mixture; the point with error bars is an experimental measurement (Peisert and Sauli, 1984). Note that, as it could be expected, both the variations due to the field and to temperature changes are minimized in the region of saturated drift velocity.

In the framework of the development of micro-pattern detectors, electron drift velocities in several gas mixtures have been measured up to very high fields, above 10 kV/cm; Figure 4.22 is an example for a mixture of helium–isobutane 80–20 at atmospheric pressure (Colas *et al.*, 2001).

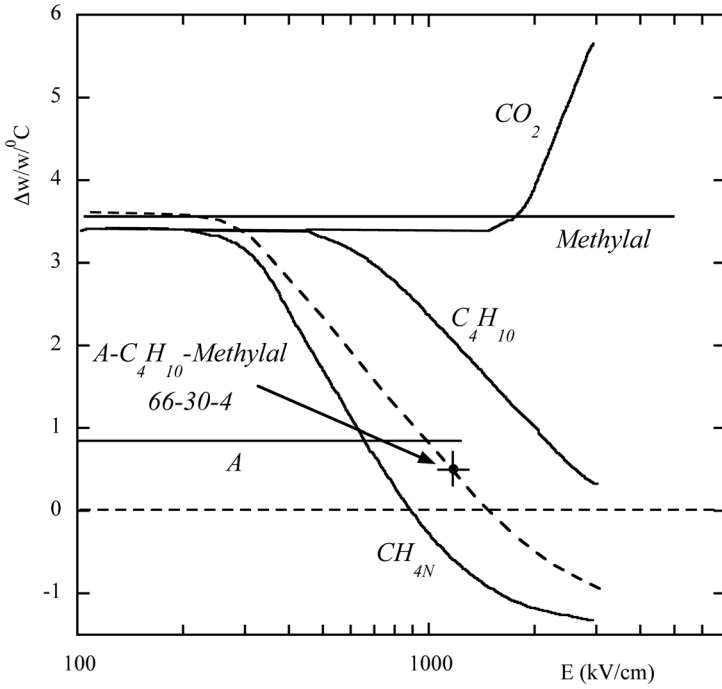


Figure 4.19 Computed variation of drift velocity as a function of field for 1 °C temperature increase (Schultz and Gresser, 1978). By kind permission of Elsevier.

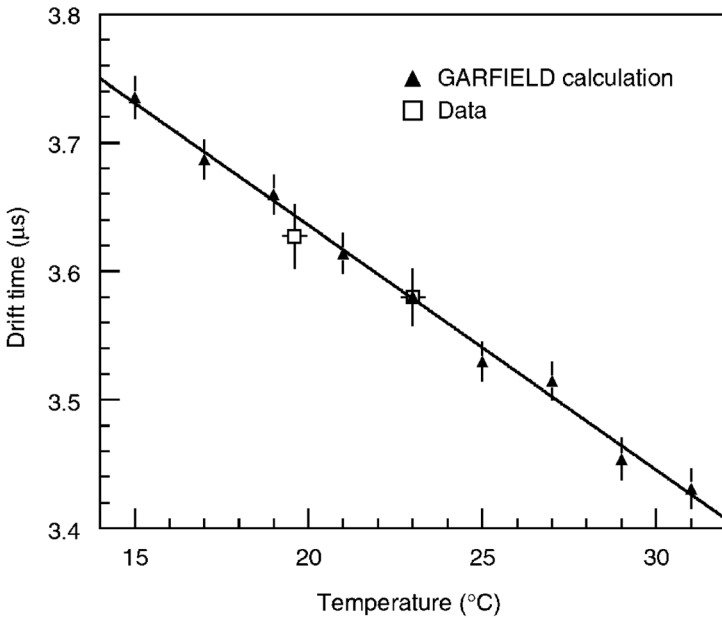


Figure 4.20 Temperature dependence of drift time for dimethyl ether at a field of 164 V/cm (Hu *et al.*, 2006). By kind permission of Elsevier.

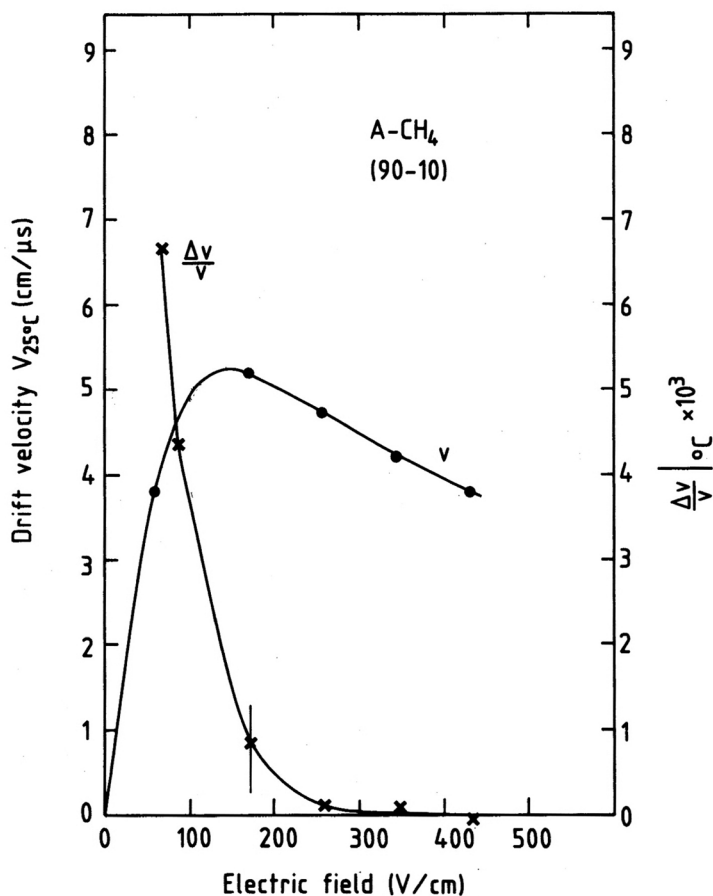


Figure 4.21 Value and temperature dependence of the drift velocity in argon-methane (Peisert and Sauli, 1984). By kind permission of CERN.

Figure 4.23 is a compilation of values of the electron linear diffusion as a function of field for several gases at NTP and 1 cm of drift (Palladino and Sadoulet, 1975). Diffusion is very large in pure noble gases, while it approaches the thermal limit in molecular gases; intermediate values are obtained for mixtures. The choice of the best gas mixture for a specific detector is often a compromise between the values of drift velocity and diffusion, and will be discussed in the following chapters.

The time expansion chamber (TEC), described in Chapter 9, relies on the use of a gas mixture having the conflicting requirements of a low diffusion, achieved at high fields, and a low drift velocity. Figure 4.24 combines measured and computed values for the mixture carbon dioxide-isobutane used in a high-resolution drift detector at DESY (Commichau *et al.*, 1985); at a field of 1 kV/cm, the drift

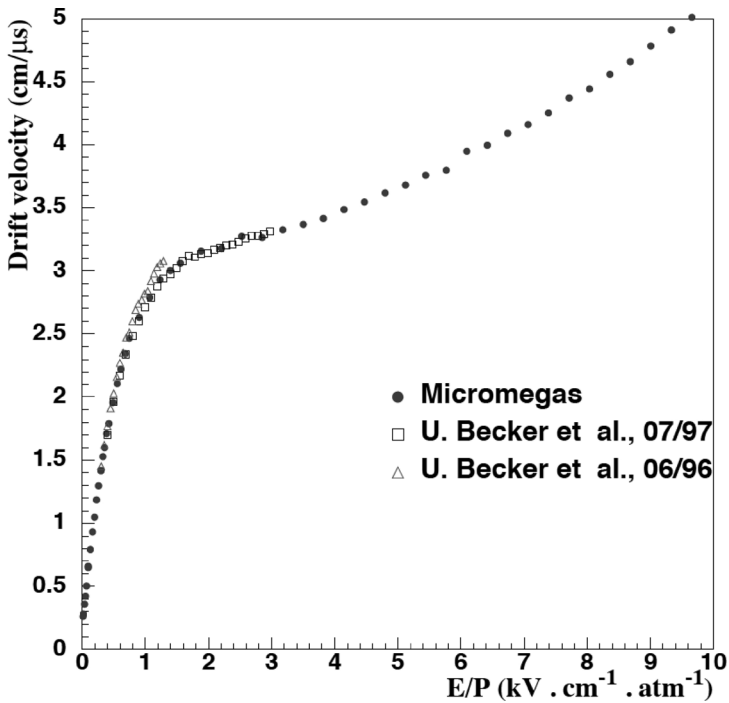


Figure 4.22 Electron drift velocity in helium–isobutane at high fields (Colas *et al.*, 2001). By kind permission of Elsevier.

velocity is around 7 $\mu\text{m}/\text{ns}$ and the diffusion is below 100 μm for 1 cm drift, very close to the thermal limit.

An interesting gas in this respect is dimethyl ether, $(\text{CH}_3)_2\text{O}$ (DME); its drift and diffusion properties are compared with other gases in Figure 4.25 and Figure 4.26 (Villa, 1983). Considered very promising in the early developments of micro-pattern gas detectors, particularly because of its non-ageing properties, it has the drawback of being flammable and chemically aggressive for some materials.

Carbon tetrafluoride also has fast drift velocity and low diffusion, comparable to methane; CF_4 -based gas mixtures for use in high-rate detectors have been studied extensively, Figure 4.27 (Christophorou *et al.*, 1979). Their main advantages for use in large volume detectors in particle physics are non-flammability and low sensitivity to neutrons; also, they do not form polymers in the avalanches, and even have etching properties capable of removing existing deposits on electrodes, as discussed in Chapter 16.

The classic theory assumes symmetric electron diffusion, described by a single coefficient D . This appeared not to be the case for some gases at high fields for which the longitudinal diffusion coefficient in the direction of drift, D_L , can be smaller than

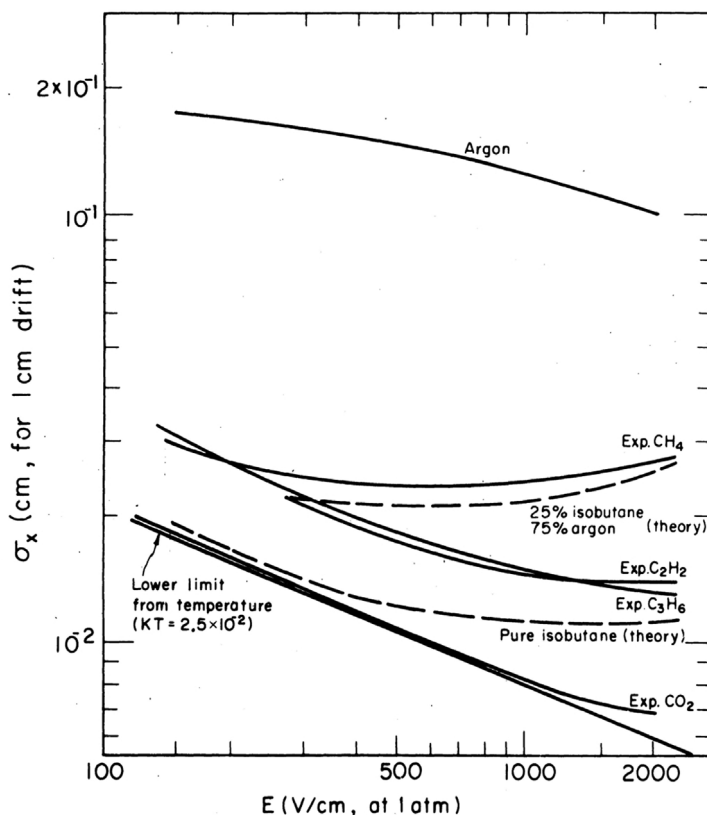


Figure 4.23 Electron diffusion (rms) for 1 cm drift in several gases (Palladino and Sadoulet, 1975). By kind permission of Elsevier.

the transverse coefficient D_T . Figure 4.28 shows the measured values of D_L/μ and D_T/μ as a function of field in argon, compared to the theoretical predictions (Lowke and Parker, 1969). In carbon dioxide, on the contrary, the diffusion remains thermal up to very high values of field, with practically no difference between longitudinal and transverse diffusion, as shown in Figure 4.29 (Christophorou, 1971). The difference can be explained by considering that the increase of electron energy between collisions is affected by the direction of the electrons in respect to the field, particularly in gases where the mean free path is long (Parker and Lowke, 1969). The reduction of longitudinal diffusion in some gas mixtures helps in improving the drift time resolution; Figure 4.30 is a measurement in an argon–methane–isobutane mixture made with the JADE detector (Drumm *et al.*, 1980).

For some gases, a violation of the E/P invariance of the drift velocity and of the inverse square root dependence on pressure of the diffusion are observed, due to a process of temporary electron capture and release from the molecules that results in slowing down of the drift at increasing pressures. Examples are given in

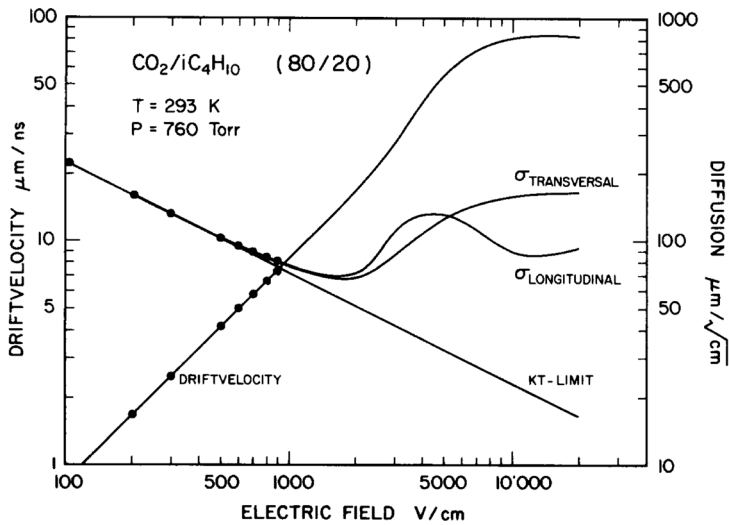


Figure 4.24 Electron drift velocity and diffusion as a function of field in $\text{CO}_2/i\text{C}_4\text{H}_{10}$ (Commichau *et al.*, 1985). By kind permission of Elsevier.

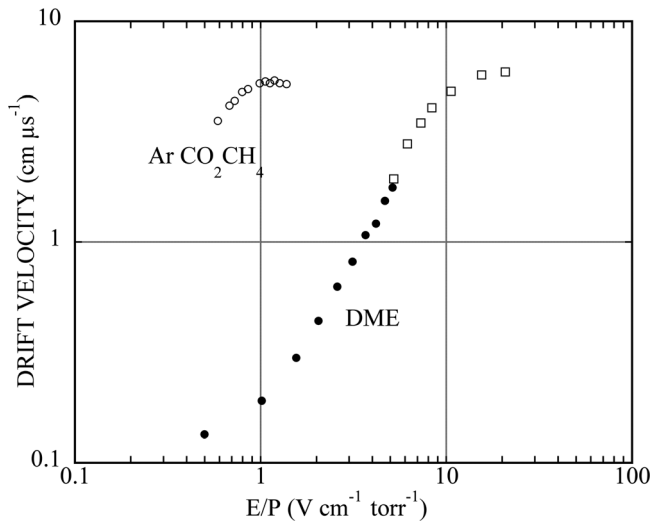


Figure 4.25 Drift velocity for 1 cm drift in DME, compared to other gases (Villa, 1983). By kind permission of Elsevier.

Figure 4.31 and Figure 4.32 for carbon dioxide (Bobkov *et al.*, 1984); a similar observation has been reported for dimethyl ether, limiting the improvement in localization accuracy that can be obtained with increasing pressures.

Figure 4.33 and Figure 4.34 are examples of measured drift velocity and Lorentz angles in a widely used drift chamber gas mixture (argon–isobutane–methylal),

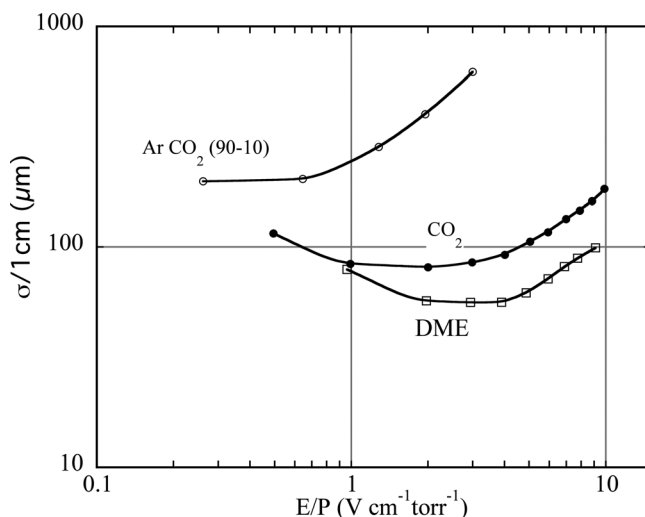


Figure 4.26 Diffusion for 1 cm drift of DME compared to other gases (Villa, 1983). By kind permission of Elsevier.

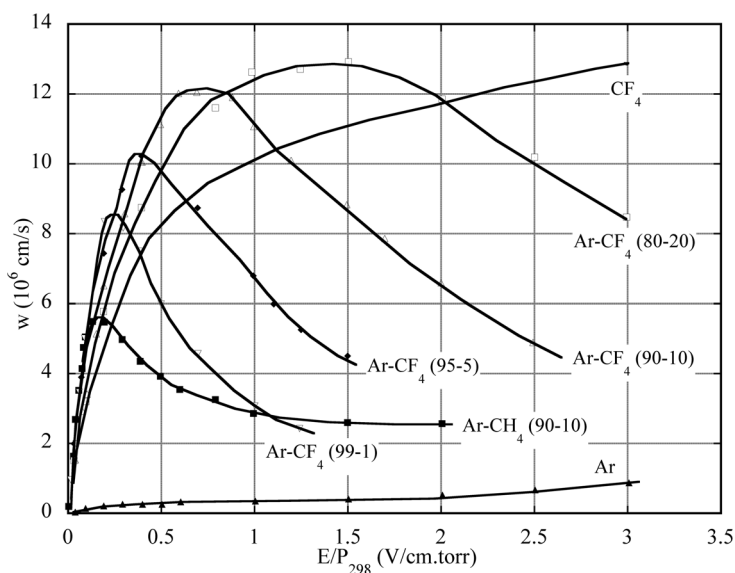


Figure 4.27 Electron drift velocity as a function of field in CF_4 , pure and in mixtures with argon (Christophorou *et al.*, 1979). By kind permission of Elsevier.

for perpendicular electric and magnetic fields (Breskin *et al.*, 1974b). The drift velocity, reduced at low electric fields, tends to reach the same saturation value for all values of magnetic field; the angle of drift follows an almost linear dependence on B for large electric fields.

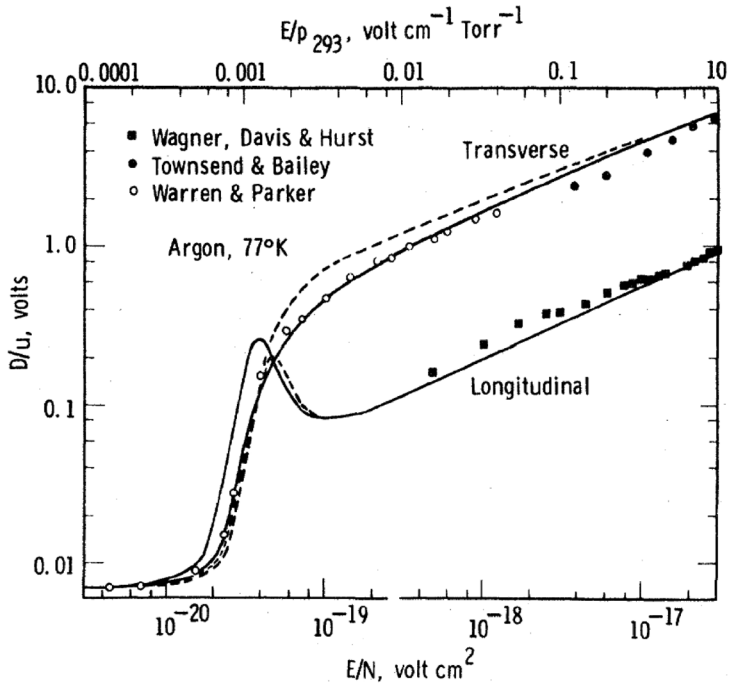


Figure 4.28 Longitudinal and transverse diffusion in argon (Lowke and Parker, 1969). By kind permission of the American Physical Society.

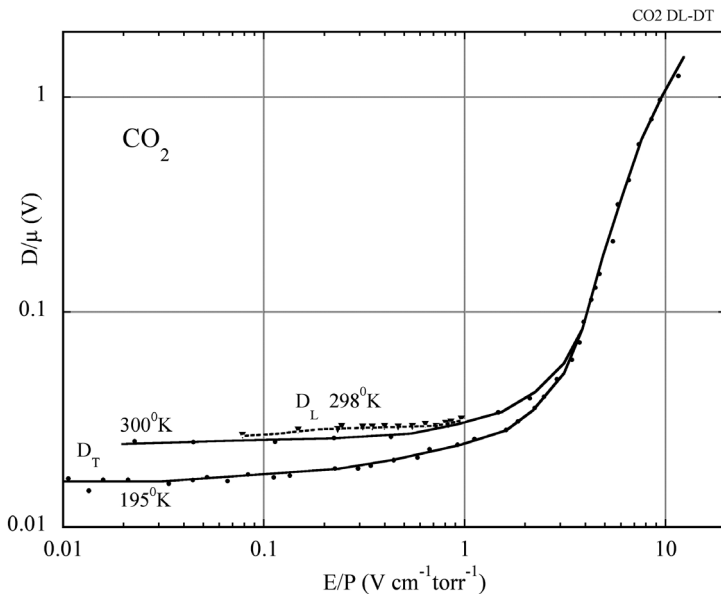


Figure 4.29 Longitudinal (D_L) and transverse (D_T) diffusion of electrons in carbon dioxide. Redrawn from data of Warren and Parker (1962) and Wagner *et al.* (1967).

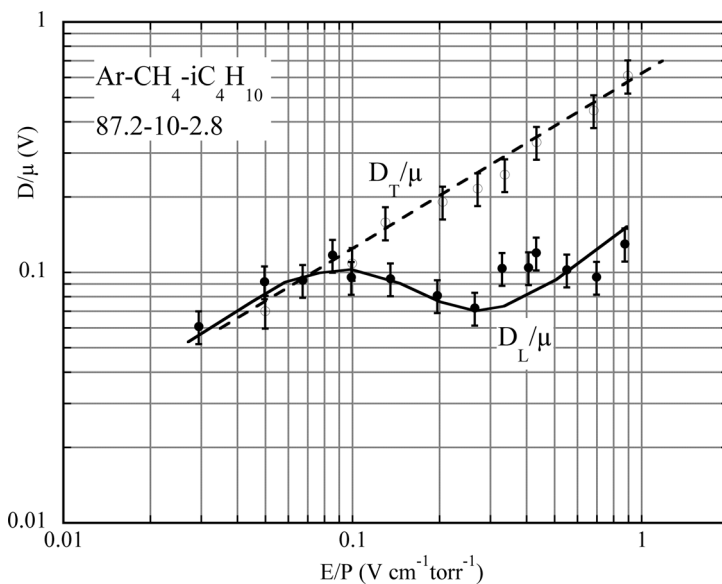


Figure 4.30 Longitudinal and transverse diffusion coefficients measured in a drift chamber (Drumm *et al.*, 1980). By kind permission of Elsevier.

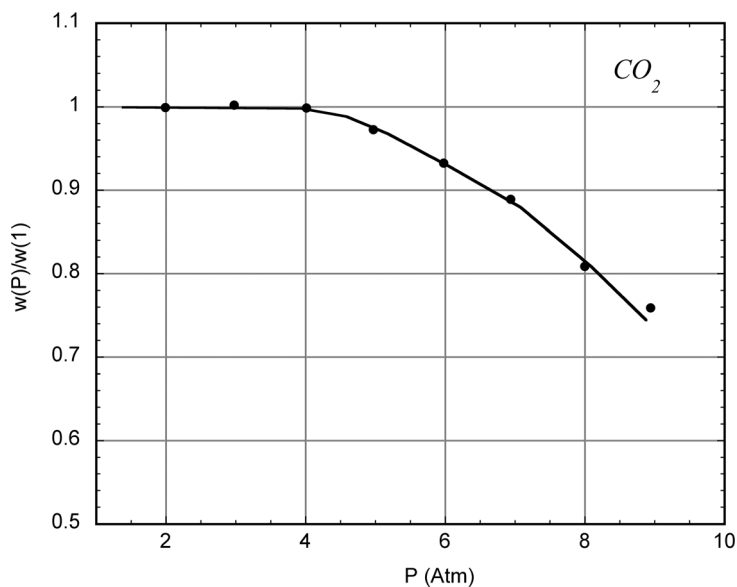


Figure 4.31 Pressure dependence of drift velocity in carbon dioxide at equal reduced field (Bobkov *et al.*, 1984). By kind permission of Elsevier.

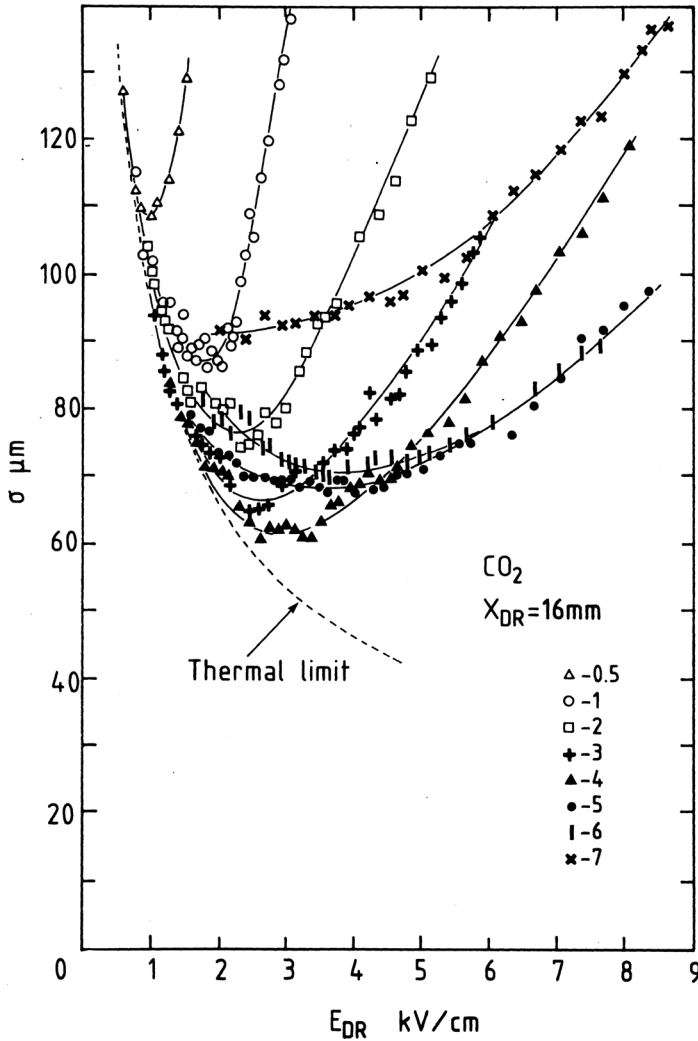


Figure 4.32 Dependence of longitudinal diffusion on the electric field for several pressures in CO₂ (Bobkov *et al.*, 1984). By kind permission of Elsevier.

While qualitatively instructive, expressions (4.17) and (4.18) are of little practical use since the dependence of τ on the fields is generally unknown. For moderate field strengths, however, one can assume that the energy distribution of electrons, and therefore the average collision time, are not affected by the field, and use Townsend's expression to deduce τ from w_0 , the measured drift velocity for $B = 0$:

$$\tau \approx \tau_0 = \frac{m}{eE} w_0; \quad (4.20)$$

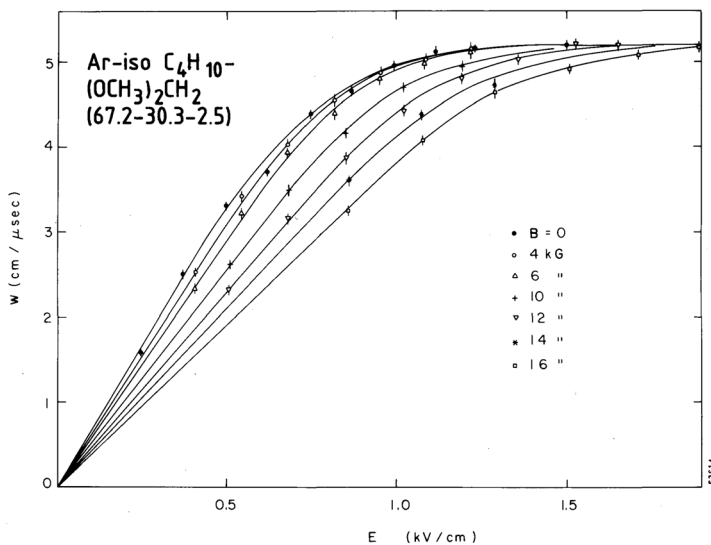


Figure 4.33 Drift velocity as a function of electric field and several values of perpendicular magnetic field (Breskin *et al.*, 1974b). By kind permission of Elsevier.

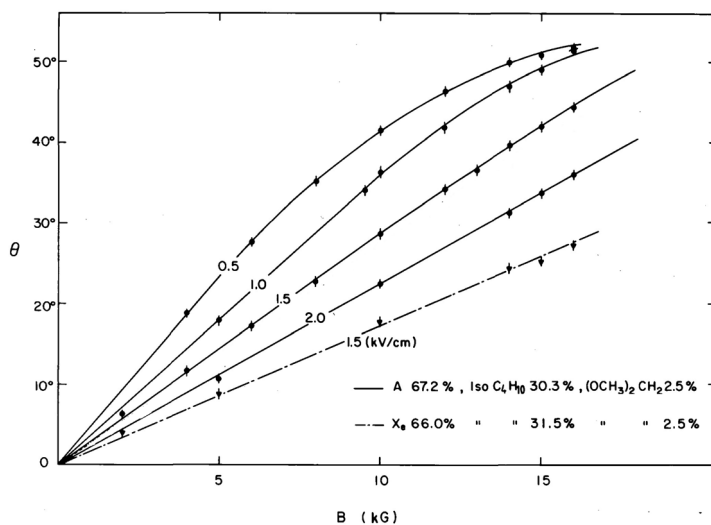


Figure 4.34 Drift angle as a function of electric and magnetic fields (Breskin *et al.*, 1974b). By kind permission of Elsevier.

magnetic drift angles and velocities can then be estimated using the quoted expressions. An example of comparison between the predictions of this simple model and measurements, for perpendicular fields, is shown in Figure 4.35 (Breskin *et al.*, 1974b); the agreement is reasonably good. At higher fields, the

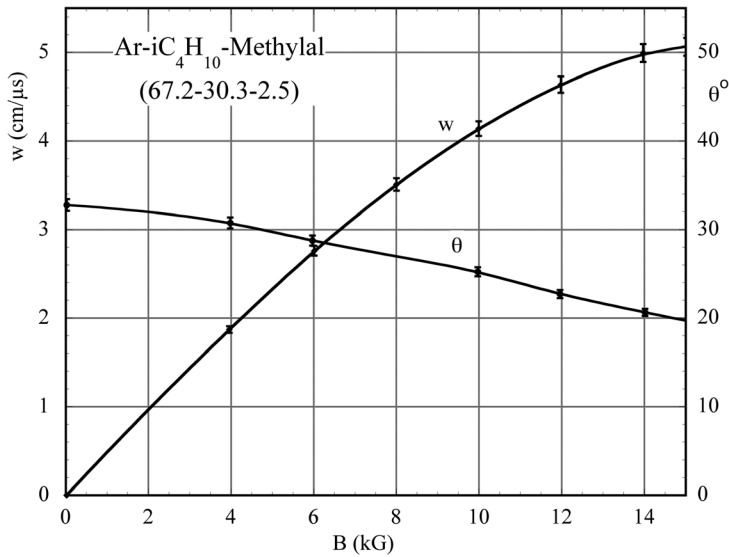


Figure 4.35 Comparison between measured values of magnetic drift velocity and angle with the predictions of a simplified model (Breskin *et al.*, 1974b). By kind permission of Elsevier.

presence of the magnetic field modifies the energy distribution of electrons and a more rigorous analysis is necessary, described in Section 4.10.

Magnetic drift velocities and Lorentz angles have been measured for many gases, in view of their relevance for detectors operated in high magnetic fields. Results for carbon tetrafluoride–isobutane and argon–carbon dioxide in equal percentage are given in Figure 4.36 (Ogren, 1995) and Figure 4.37 (Bittl *et al.*, 1997), and for a mixture of several gases with dimethyl ether in Figure 4.38 (Angelini *et al.*, 1994). Other measurements in a range of fast gas mixtures are reported in Kiselev *et al.* (1995) and confirm the general property of ‘cold’ gases, where electrons remain close to thermal at high fields, to have small magnetic angles.

With the availability of computer programs permitting one to calculate drift and diffusion properties in a wide range of gases and their mixtures the interest in systematic measurements of drift properties has decreased, although an experimental verification is often needed for special conditions.

4.8 Electron capture

Drifting in the gas under the effect of an electric field, electrons can be captured by molecules with electronic affinity creating negative ions. The major capture process, resonance dissociative attachment, has been abundantly described in the

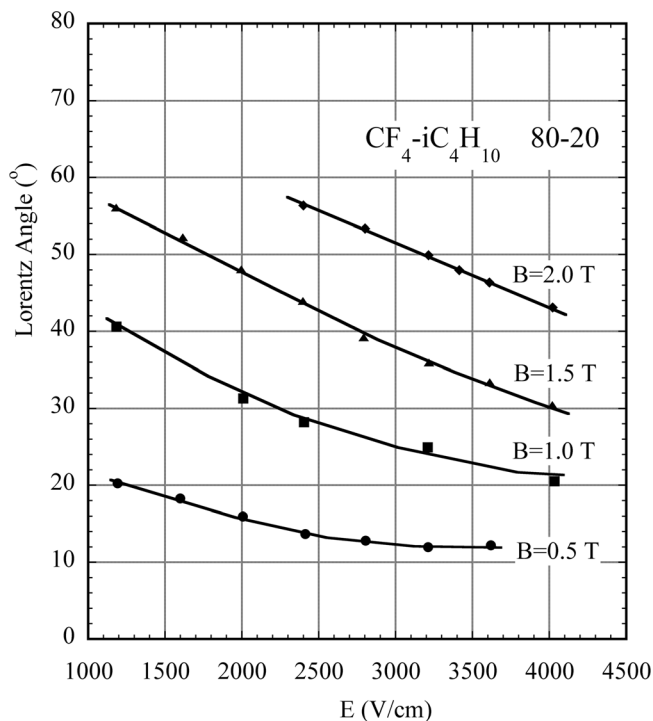


Figure 4.36 Lorentz angle as a function of perpendicular electric and magnetic fields in a $\text{CF}_4\text{-iC}_4\text{H}_{10}$ 80–20 (Ogren, 1995). By kind permission of Elsevier.

literature, see for example Christophorou (1971); modern theories of electron transport include the capture cross sections in the estimate of drift properties.

In the classic theory (Brown, 1959), the capture process can be described by defining an attachment coefficient h , the probability of attachment per collision. The number of electron–molecule collisions per unit drift length is given by $(w\tau)^{-1}$, where w and τ are the drift velocity and mean collision time. Introducing Townsend's expression (4.13), the number of collisions with attachment per unit drift length is:

$$h \frac{1}{w\tau} = h \frac{e E}{m w^2},$$

the electron loss during drift is then described by the differential equation:

$$dn = - \frac{e E}{m w^2} dx;$$

an integration provides the number of surviving electrons after a drift length s :

$$n = n_0 e^{-\frac{e E s}{m w^2}} = n_0 e^{-\frac{s}{\lambda}}, \quad (4.21)$$

where λ is a phenomenological mean capture length.

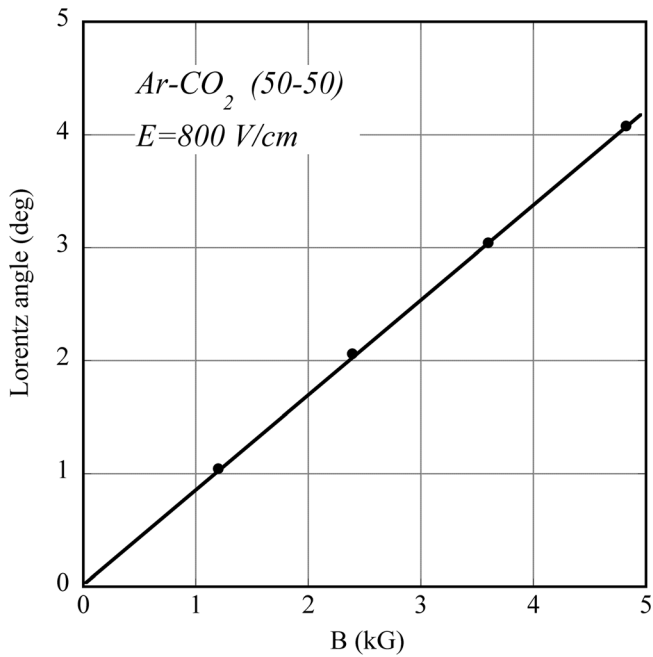


Figure 4.37 Lorentz angle as a function of perpendicular electric and magnetic fields in Ar-CO₂ 50–50 (Bittl *et al.*, 1997). By kind permission of Elsevier.

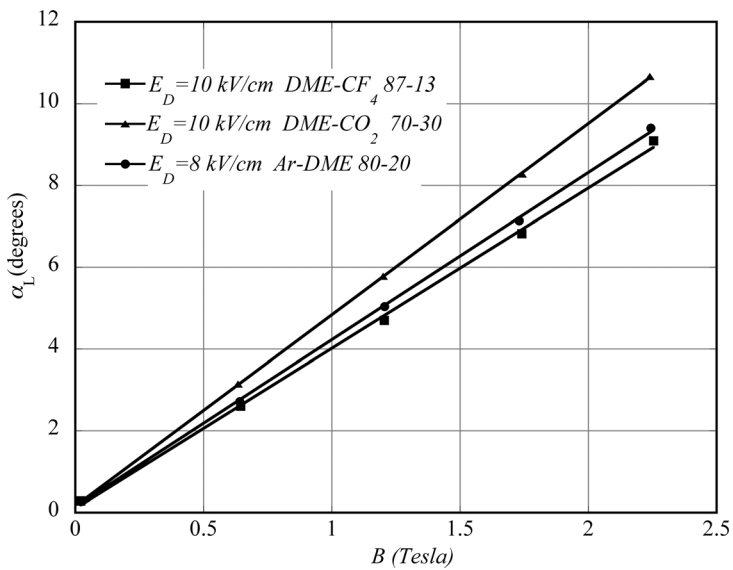


Figure 4.38 Lorentz angle in DME mixtures (Angelini *et al.*, 1994). By kind permission of Elsevier.

With the addition to a main gas of electro-negative molecules in a percentage p , and assuming that neither the drift velocity nor the attachment coefficient are modified, the previous expression can be written as:

$$n = n_0 e^{-ps/\lambda}. \quad (4.22)$$

For a detector uniformly exposed to radiation, with a drift cell size S , and assuming that the capture length is not affected by field variations within the cell, the average collected charge, normalized to the initial ionization charge, can be obtained by integrating the previous expression over the full drift path length S :

$$\frac{Q_S}{Q_0} = \int_0^S e^{-ps/\lambda} ds = \frac{\lambda}{P} \left(1 - e^{-ps/\lambda} \right). \quad (4.23)$$

As the detected charge fraction depends on the drift length within the cell, the energy resolution will of course be correspondingly affected.

Values of attachment coefficients for several gases, in the absence of an electric field, were given in Table 4.3. The cross section for electron capture varies considerably, however, with the electron energy, hence the field, and has been extensively studied experimentally, particularly for thermal electron energies; classic examples are given for oxygen in Figure 4.39 (Bloch and Bradbury, 1935) and for water in Figure 4.40 (Bradbury and Tatel, 1934). In both cases, the attachment probability is large for low fields and electron energies close to thermal, but decreases at increasing fields; for water, it becomes negligible at fields of a few $\text{Vcm}^{-1}\text{torr}^{-1}$.

Figure 4.41 is a collection of values of attachment rate as a function of electron energy for chlorinated vapours (Christodoulides and Christophorou, 1971); while usually not intentionally present as constituents in the main gas mixture, these compounds are often used as cleaning agents during the detector construction, and special care should be taken to remove these residual contaminations.

Modern compilations and measurements of the electron–molecule cross sections, including capture, and their relevance in the detectors' performances will be discussed in Section 4.10.

As discussed in the next section, due to the field dependence of electron–molecules cross sections, their energy distribution at a given value of field depends on the gas or gas mixture; as a consequence, the capture probability can differ considerably in different mixtures, for equal amounts of electro-negative contaminants. This is seen in Figure 4.42, where the experimentally measured fractions of electrons surviving after a 20 cm drift in a detector, at a drift field of 200 V/cm , are given as a function of oxygen content for two gas mixtures. For equal oxygen

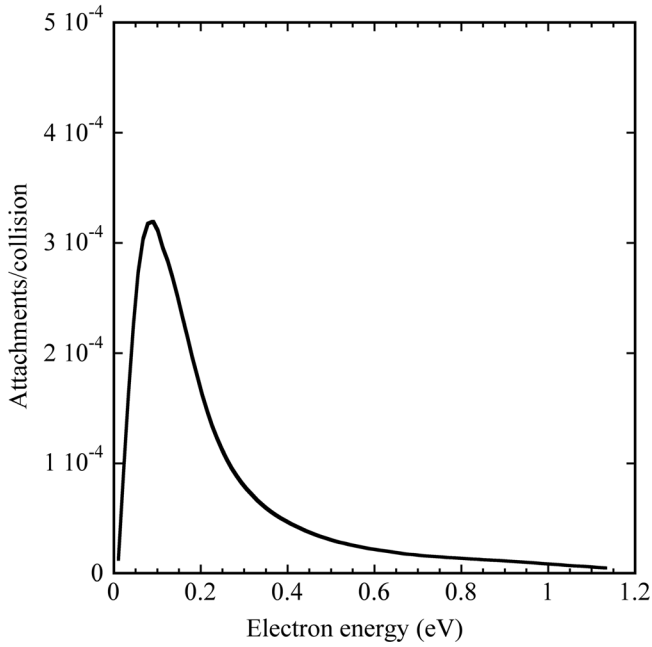


Figure 4.39 Electron attachment coefficient for oxygen (Bloch and Bradbury, 1935).

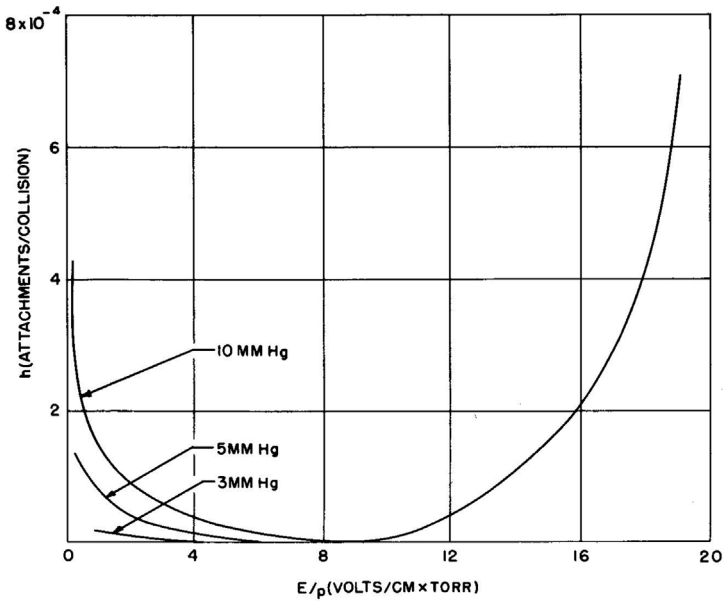


Figure 4.40 Electron capture probability in water vapours as a function of reduced field (Bradbury and Tatel, 1934).

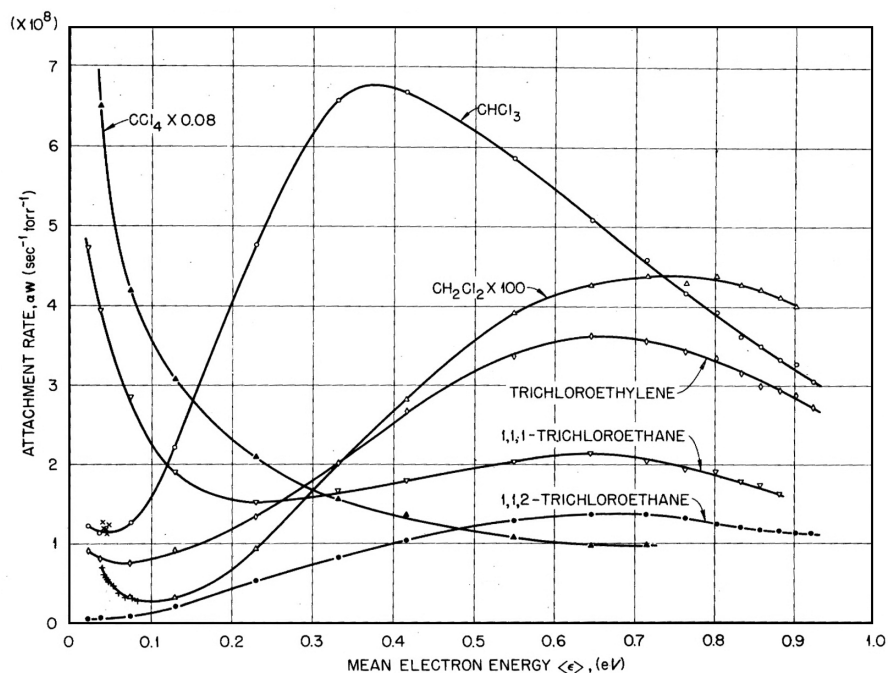


Figure 4.41 Attachment rates of chlorinated vapours (Christodoulides and Christophorou, 1971). By kind permission of the American Institute of Physics.

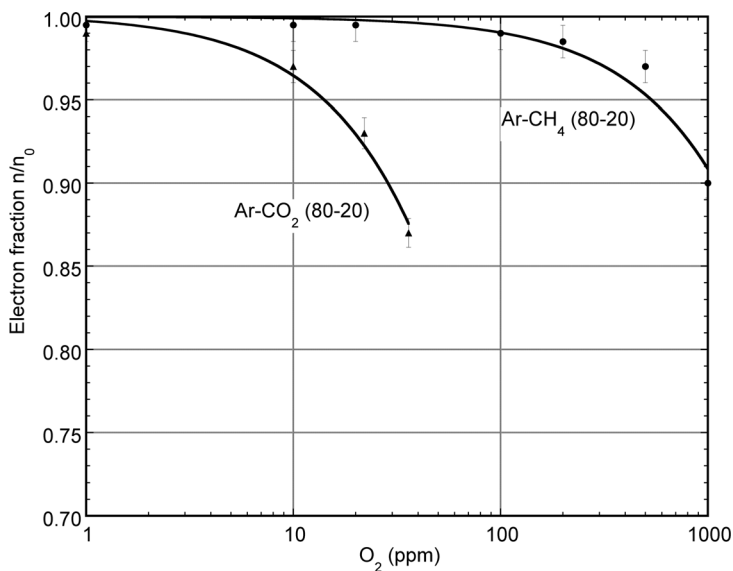


Figure 4.42 Fraction of electrons surviving after 20 cm drift in two gas mixtures, as a function of oxygen content ($E = 200$ V/cm). Compilation from Ar-CO₂ data of Price *et al.* (1982) and Ar-CH₄ data of Lehraus *et al.* (1984).

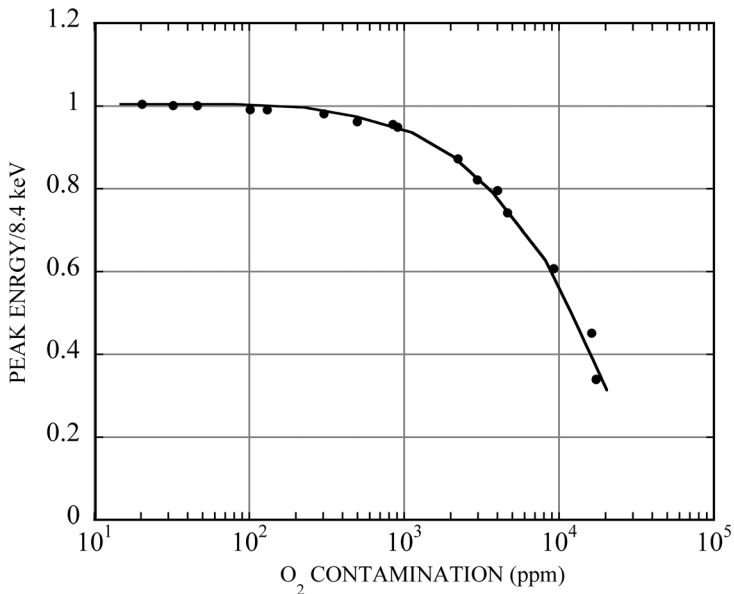


Figure 4.43 Ionization capture losses in a drift chamber as a function of oxygen content in a xenon–methane 90–10 mixture (Chiba *et al.*, 1988). By kind permission of Elsevier.

content, in argon–carbon dioxide (Price *et al.*, 1982), where electrons remain thermal up to very high values of field, the capture losses are much larger than for argon–methane mixtures, in which the average electron energy is increased well above thermal by the field (Lehraus *et al.*, 1984). The full lines are an exponential fit to the measurements with expression (4.22), using suitable values of the parameters.

The results of measurements of ionization energy loss in a charged particles beam uniformly illuminating a detector with 1 cm drift in a xenon–methane gas mixture are shown in Figure 4.43; the curve is a fit to the data with $\lambda p = 7.8 \times 10^{-3}$ (Chiba *et al.*, 1988). Similar studies, aiming at finding the effect of residual oxygen and SF₆ contaminations in xenon-filled drift chambers, demonstrate the crucial role of the electric field strength in determining the energy of the electrons and the ensuing capture losses. Figure 4.44 is an example of measured pulse height distributions for soft X-rays at several values of drift field (Andronic *et al.*, 2003).

4.9 Electron drift in liquid noble gases

Drift velocity and diffusion of electrons in liquefied noble gases have been studied years ago. The major difficulty both for measurements and exploitation in detectors

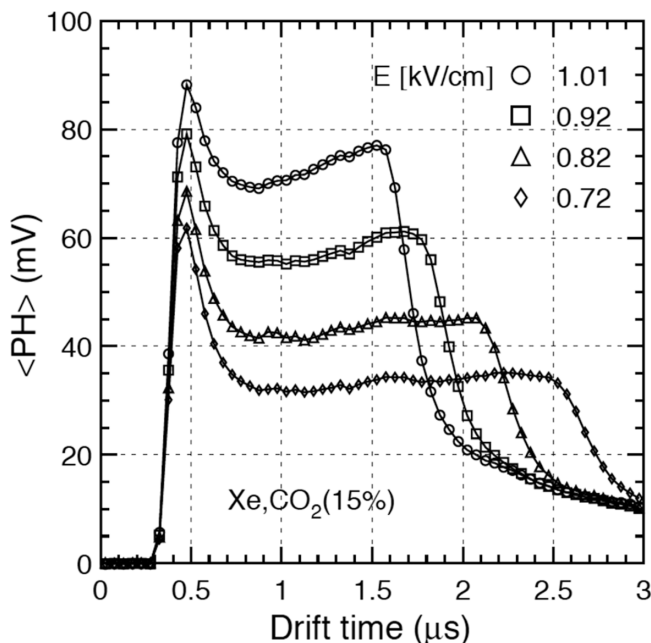


Figure 4.44 Average pulse height as a function of drift time for several values of drift field (Andronic *et al.*, 2003). By kind permission of Elsevier.

lies in the extreme sensitivity of the electron drift to the gas purity and the presence of electro-negative contaminations, often expresses in terms of electron lifetimes; this explains discrepancies between measurements. Figure 4.45, an eye-fit compilation from data from Miller *et al.* (1968), provides the electron drift velocity in liquid argon, krypton and xenon; at comparable values of field, the drift velocities are about ten times lower than in the corresponding gas phase.

The electron drift in liquid argon and xenon has been studied systematically in the course of development of the cryogenic and dual-phase detectors, described in Section 15.2. Measured with an LAr-TPC prototype, Figure 4.46 shows the field dependence of the velocity at two temperature values; measurements are compared with an empirical expression (Walkowiak, 2000). Figure 4.47 is the field dependence of electron drift velocity for xenon (Aprile *et al.*, 1991); experimental values of electron diffusion in liquid argon and xenon as a function of the reduced field E/N are given in Figure 4.48 (Doke, 1982).

For applications requiring charge multiplication in the gas phase, small additions of methane permit one to reach higher gains and faster drift velocity, with only a small reduction of the scintillation yield; electron drift properties in a double-phase xenon cell with small methane concentrations are described in (Lightfoot *et al.* (2005).

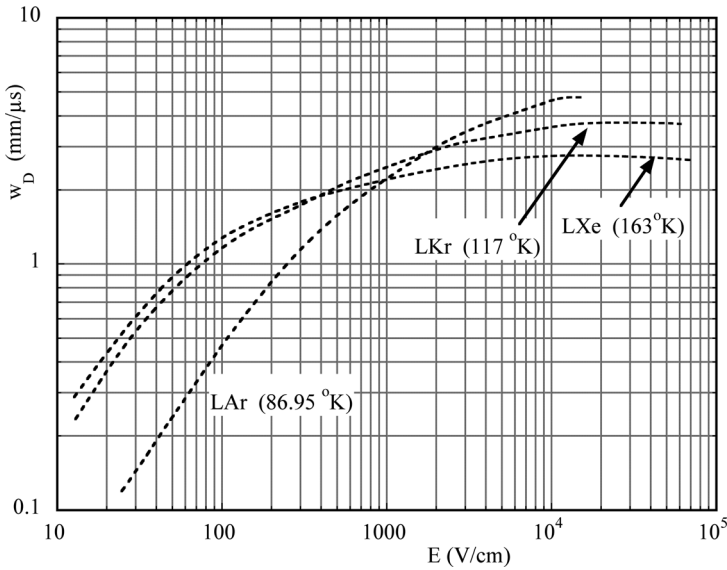


Figure 4.45 Electron drift velocity in liquid noble gases. Data from Miller *et al.* (1968).

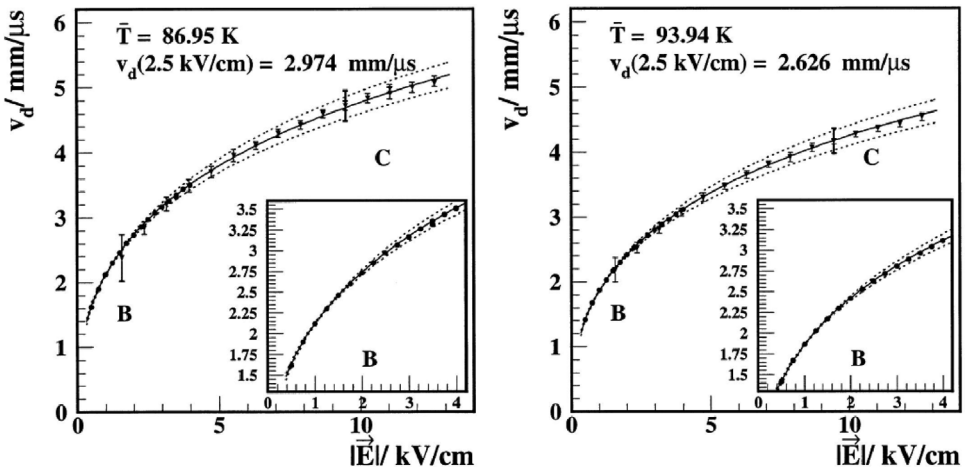


Figure 4.46 Electron drift velocity in liquid argon at two values of temperature (Walkowiak, 2000). By kind permission of Elsevier.

4.10 Transport theory

A rigorous theory of electron drift in gases has been developed by many authors, based on seminal works on Boltzmann transport theory describing the behaviour of free electrons in a gas under the influence of an electric field (Morse *et al.*, 1935). The algorithm can be outlined as follows: at each value of the field, the

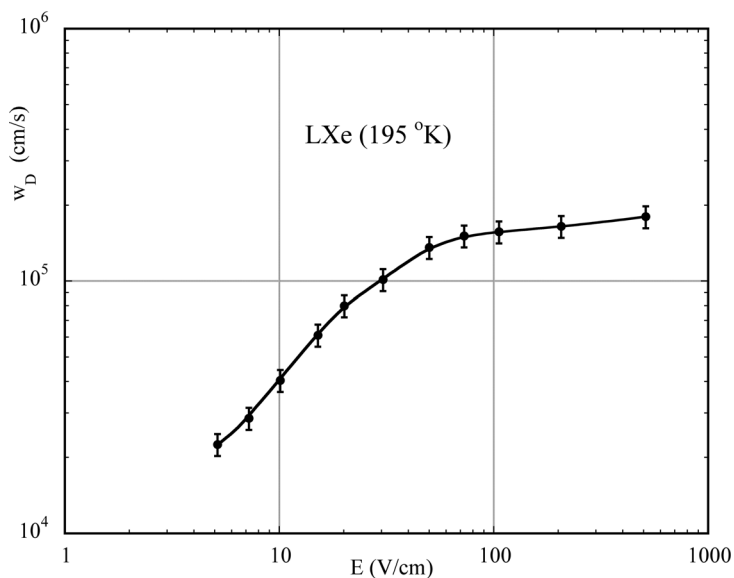


Figure 4.47 Electron drift velocity in liquid xenon (data from Aprile *et al.*, 1991). By kind permission of Elsevier.

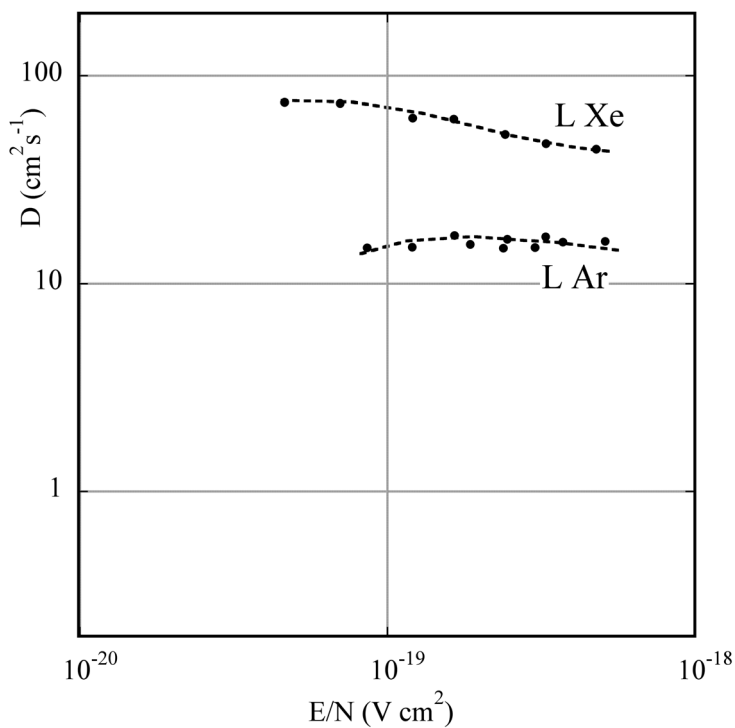


Figure 4.48 Electron diffusion in liquid argon and xenon (data from Doke, 1982). By kind permission of Elsevier.

energy distribution of electrons is computed by equalizing the energy gained from the field to that lost in collisions with the molecules; the calculation takes into account the energy-dependent values of electron–molecule cross sections, both elastic and inelastic. Once the energy distribution is known, the various drift and diffusion properties can be deduced. The theory was revived in the eighties in the study of drift chamber performances (Palladino and Sadoulet, 1975; Schultz and Gresser, 1978; Schultz, 1976; Biagi, 1999); a dedicated software program, MAGBOLTZ, is extensively used to compute drift and diffusion properties of electrons in a wide range of gases and gas mixtures (Biagi and Veenhof, 1995b).

Under rather broad assumptions, and for fields such that only a negligible fraction of the electrons get enough energy to experience ionizing collisions, one can deduce the following expression for the energy distribution:

$$F_0(\varepsilon) = C\sqrt{\varepsilon} e^{-\int \frac{3\varepsilon \Lambda(\varepsilon) d\varepsilon}{[e E l(\varepsilon)]^2}}, \quad (4.24)$$

with the mean free path between collisions given by:

$$l(\varepsilon) = \frac{1}{N\sigma(\varepsilon)}, \quad (4.25)$$

where N is the number of molecules per unit volume (Avogadro's number) and $\sigma(\varepsilon)$ is the electron–molecule cross section at the electron energy ε ; $\Lambda(\varepsilon)$ represents the fractional energy loss in the collisions. For an ideal gas at absolute temperature T and pressure P (in mmHg), N is given by:

$$N = 2.69 \times 10^{19} \frac{P}{760} \frac{273}{T}. \quad (4.26)$$

Appropriate terms can be added to the expression (4.24) to take into account inelastic collisions (excitation, ionization), described by the respective cross sections (Palladino and Sadoulet, 1974).

If the elastic and inelastic cross sections are known, $F_0(\varepsilon)$ can be computed numerically, and the drift velocity and diffusion coefficient are obtained from the expressions:

$$\begin{aligned} w(E) &= \frac{2}{3} \frac{e}{m} E \int \varepsilon l(\varepsilon) \frac{\partial F_0(\varepsilon)}{\partial \varepsilon} d\varepsilon, \\ D(E) &= \int \frac{l(\varepsilon)}{3} v F_0(\varepsilon) d\varepsilon, \end{aligned} \quad (4.27)$$

where $v = \sqrt{2\varepsilon/m}$ is the instant velocity of electrons of energy ε . Simple composition rules hold for gas mixtures, with obvious meanings:

$$\sigma(\varepsilon) = \sum p_i \sigma_i(\varepsilon) \quad \text{and} \quad \sigma(\varepsilon)\Lambda(\varepsilon) = \sum p_i \sigma_i(\varepsilon)\Lambda_i(\varepsilon).$$

It is customary to define a characteristic energy ε_k as follows:

$$\varepsilon_k = \frac{e E D(E)}{w(E)}; \quad (4.28)$$

a comparison with expression (4.9) shows that the characteristic energy replaces the factor kT , and represents the average ‘heating’ of the electron swarm by the field. Further refinements in the theory and computational algorithms permit one to take into account the non-symmetric diffusion and the effect of the magnetic field on drifting electron swarms (Biagi, 1999).

The electron–molecule collision cross sections depend very strongly on E for most gases; for argon they go through maxima and minima (the Ramsauer effect). This is a consequence of the fact that the electron wavelengths approach those of the electron shells of the atom or molecule, and complex quantum-mechanical processes take place. At increasing values of E , the energy distribution therefore changes from the original Maxwellian shape, and the average energy can exceed the thermal value by orders of magnitude; eventually, cross sections reach a minimum, resulting in a saturation and even decrease of the drift velocity at increasing field.

The program MAGBOLTZ includes extensive compilations of the electron–molecule cross sections for a wide list of gases (Biagi and Veenhof, 1995a); detailed and updated values for the electron–molecule cross sections can be found on the open-access web site LXCAT. Figure 4.49 to Figure 4.54, simplified plots from the numerical data provided by LXCAT from the Morgan compilation (Montgomery and Montgomery, 1941) give examples for several atomic and molecular gases. For noble gases, the cross section is elastic until the electrons reach the first excitation and ionization energy, above 10 eV; on the contrary, for molecular gases inelastic channels, vibrational and rotational cross sections open up at energies above 0.1 eV. For electro-negative species, the attachment cross section is also given; in oxygen, a peak between 0.06 and 0.1 eV explains the large electron capture probability near thermal energies. Carbon tetrafluoride, on the contrary, has a peak around 8 eV, causing electron losses at high field values.

High values of the cross sections reduce the electron diffusion and increase the drift velocity; a large inelasticity implies that high fields are required to raise the electron energy. One can also understand why the addition of very small

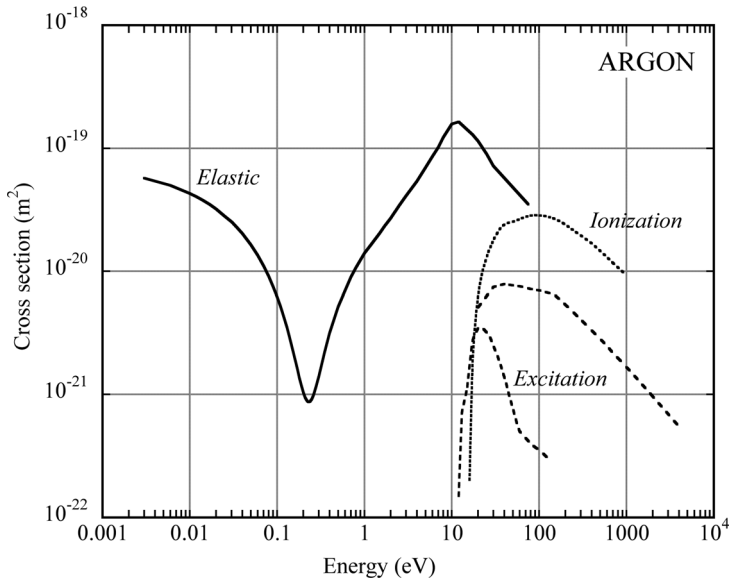


Figure 4.49 Electron–molecule cross section for argon (data from LXCAT).

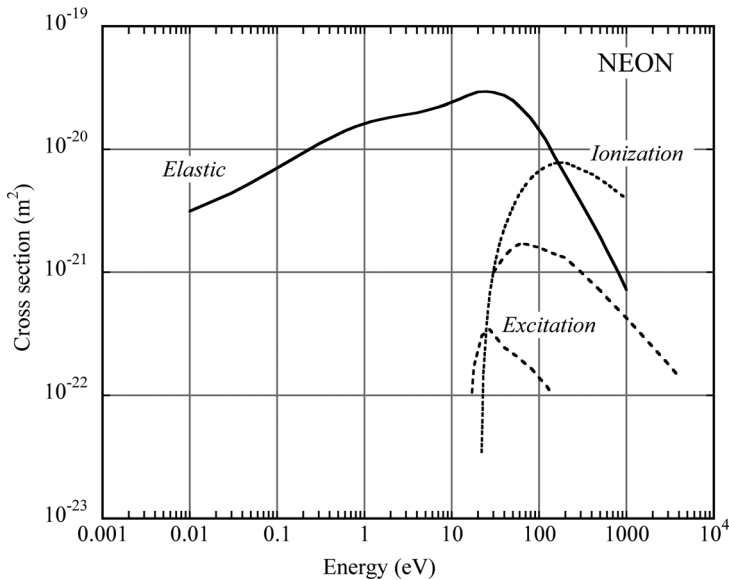


Figure 4.50 Electron–molecule cross section for neon (data from LXCAT).

amounts of a molecular gas to noble gases has the observed large effect on drift properties: for argon, at an energy close to the Ramsauer minimum, a 1% addition of carbon dioxide results in equal contributions to the cross sections of the two species.

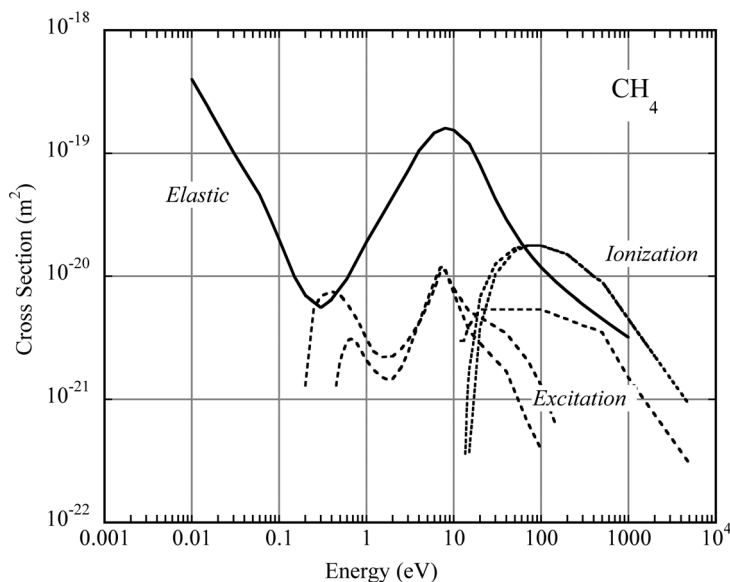


Figure 4.51 Electron–molecule cross section for methane (data from LXCAT).

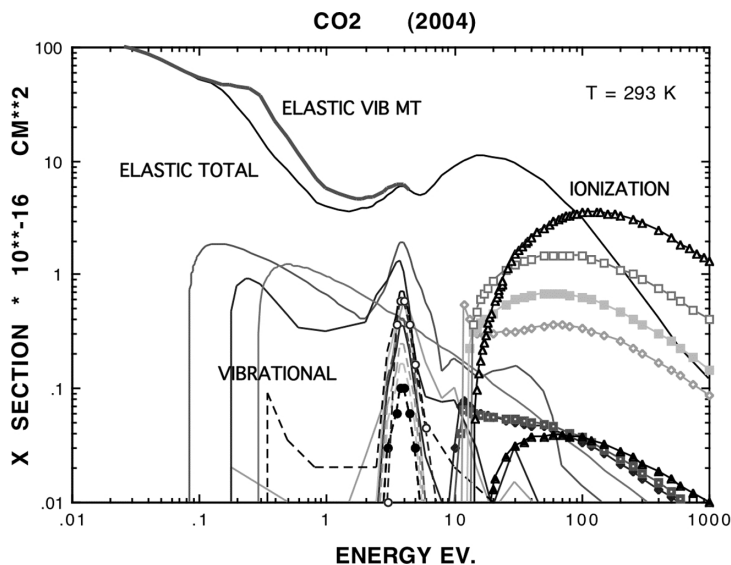


Figure 4.52 Electron–molecule cross section for carbon dioxide (data from LXCAT).

The predictive accuracy of the program has been verified in many cases when accurate data are available; Figure 4.55 and Figure 4.56 (Biagi, 1999) give representative examples.

Figure 4.57 shows the computed electron energy distribution at moderate fields (100 V cm^{-1}) in pure argon and in a 70–30 mixture of argon and carbon dioxide at

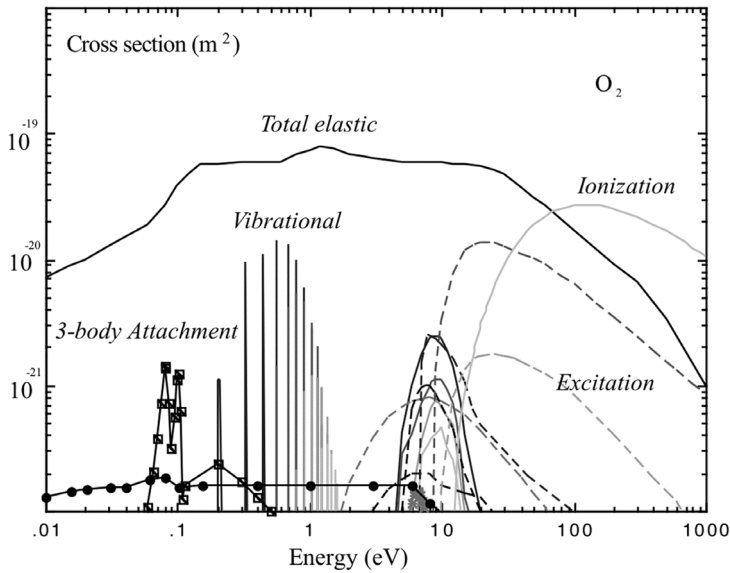


Figure 4.53 Electron–molecule cross section for oxygen (data from LXCAT).

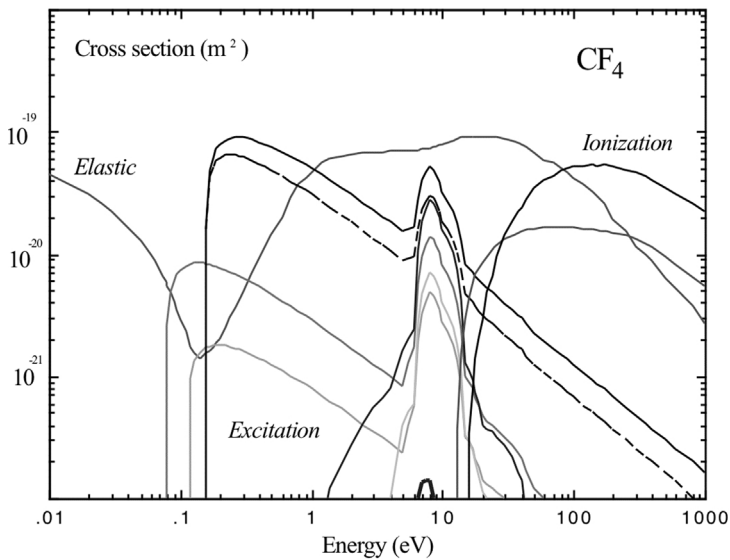


Figure 4.54 Electron–molecule cross section for carbon tetrafluoride (data from LXCAT).

NTP; the already mentioned ‘cooling’ effect of the addition of a molecular gas is apparent, with an average electron energy close to the thermal value for the mixture, while it reaches several eV in pure argon.

The electron energy is increased towards larger values with the application of higher electric fields. An example of computed distributions for an

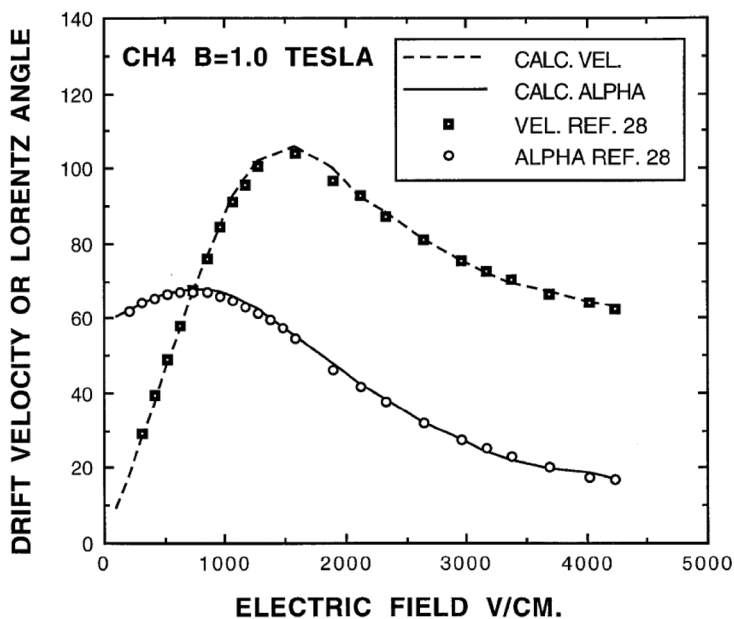


Figure 4.55 Computed and measured electron drift velocity in methane (Biagi, 1999). By kind permission of Elsevier.

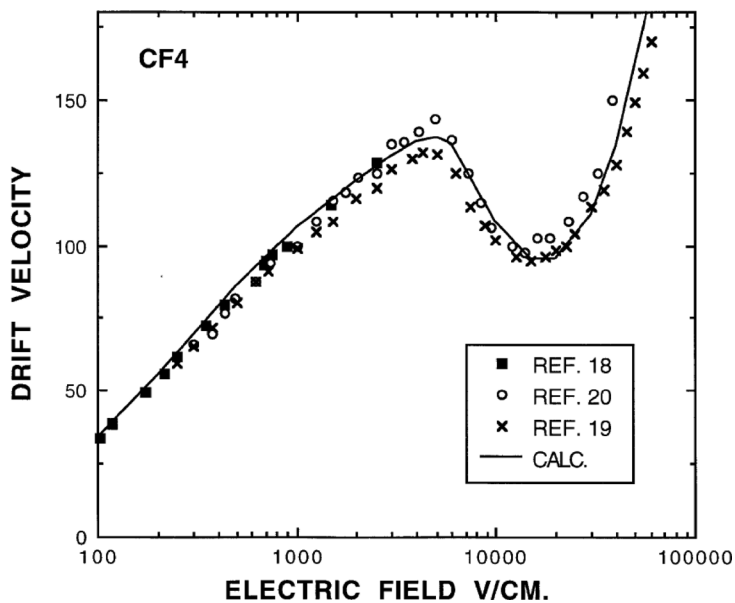


Figure 4.56 Computed and measured electron drift velocity in carbon tetrafluoride (Biagi, 1999). By kind permission of Elsevier.

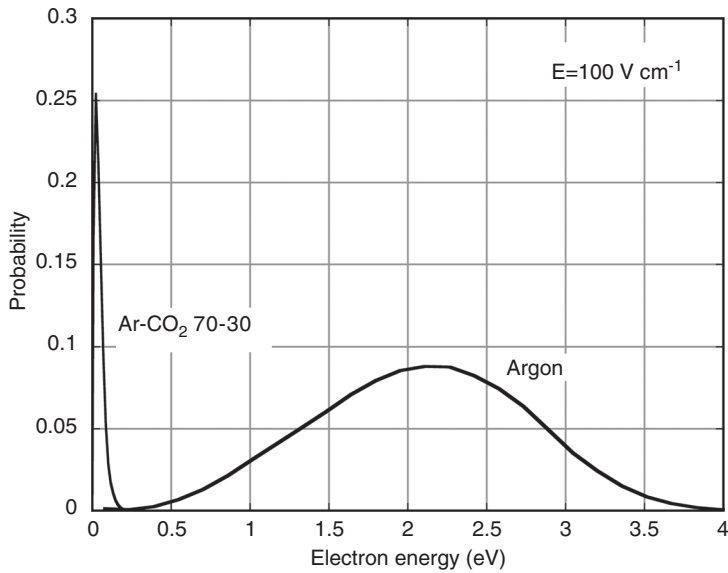


Figure 4.57 Computed electron energy distribution for pure argon and argon-CO₂ at low fields.

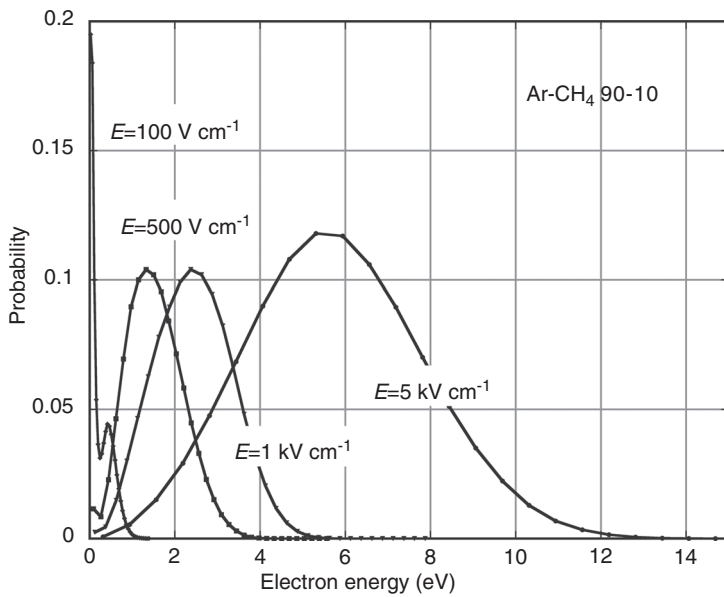


Figure 4.58 Computed electron energy distribution as a function of field in argon-CH₄.

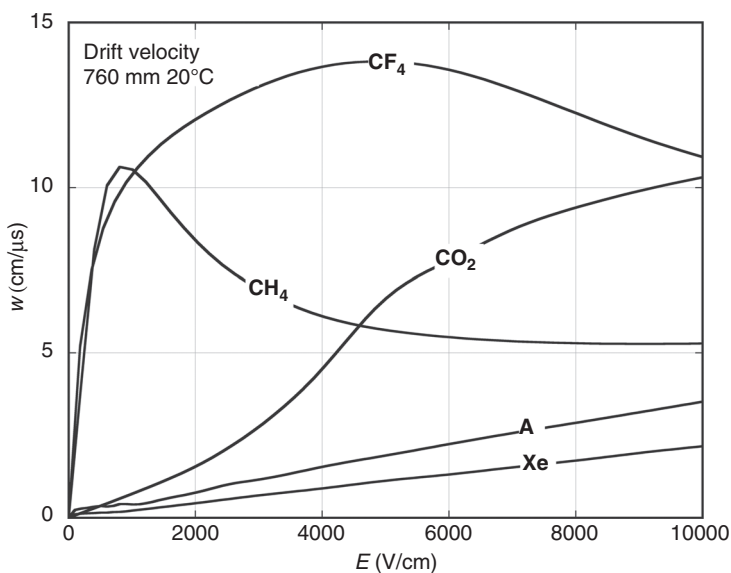


Figure 4.59 Computed drift velocity as a function of field for pure gases at NTP.

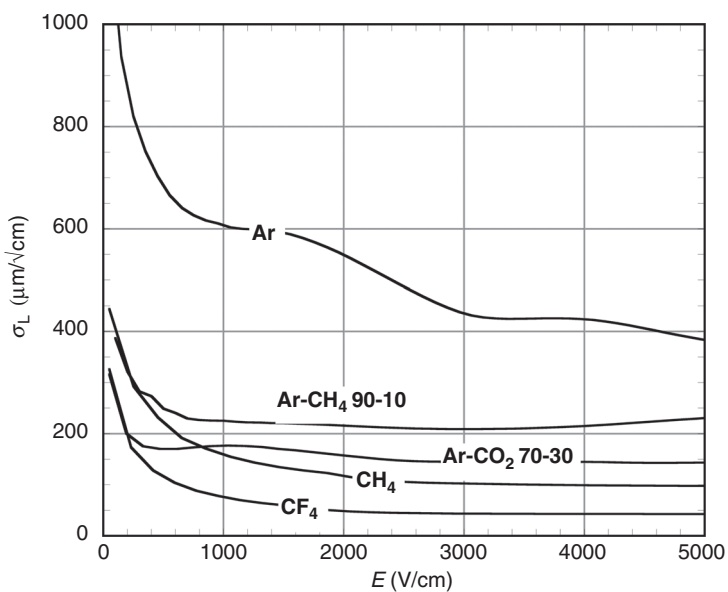


Figure 4.60 Computed longitudinal diffusion for 1 cm drift in several gases at NTP.

argon–methane 90–10 mixture at NTP is given in Figure 4.58; for a field of 5 kV cm^{-1} the upper tail of the distributions exceeds the inelastic excitation and ionization levels of methane (8.8 and 12.6 eV, respectively), causing the onset of inelastic processes.

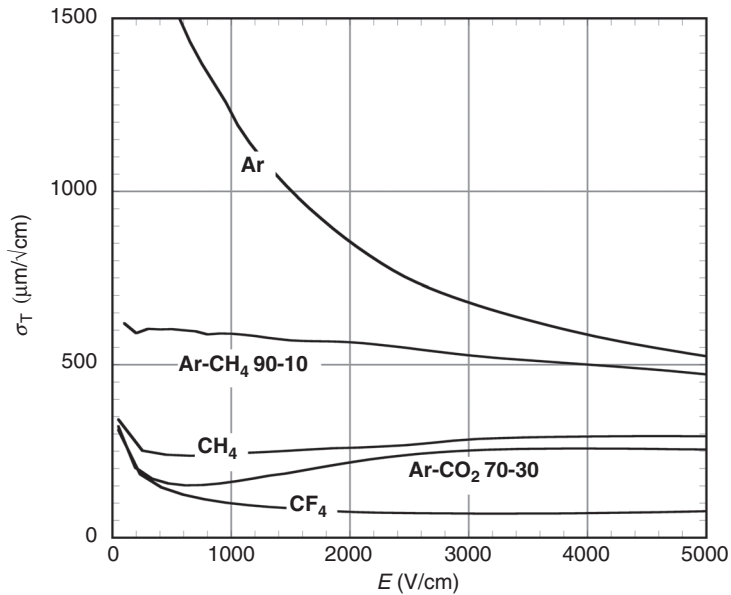


Figure 4.61 Computed transverse diffusion for 1 cm of drift in several gases at NTP.

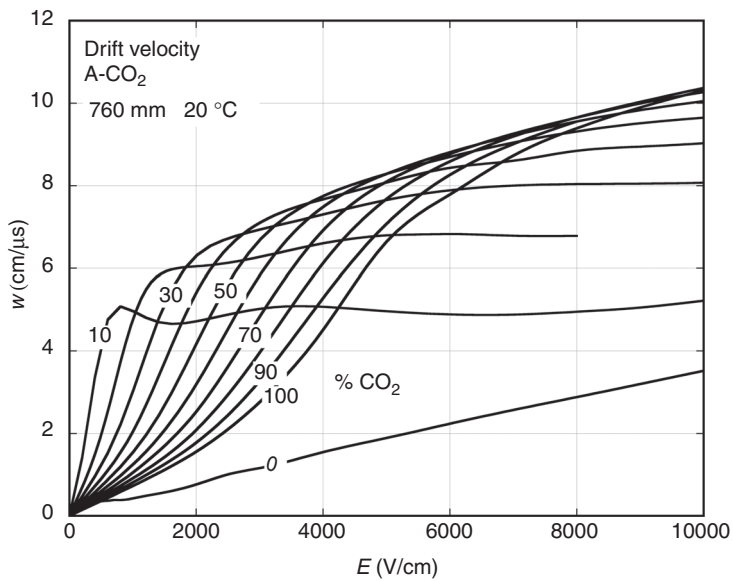


Figure 4.62 Computed drift velocity as a function of field for argon-carbon dioxide mixtures at NTP.

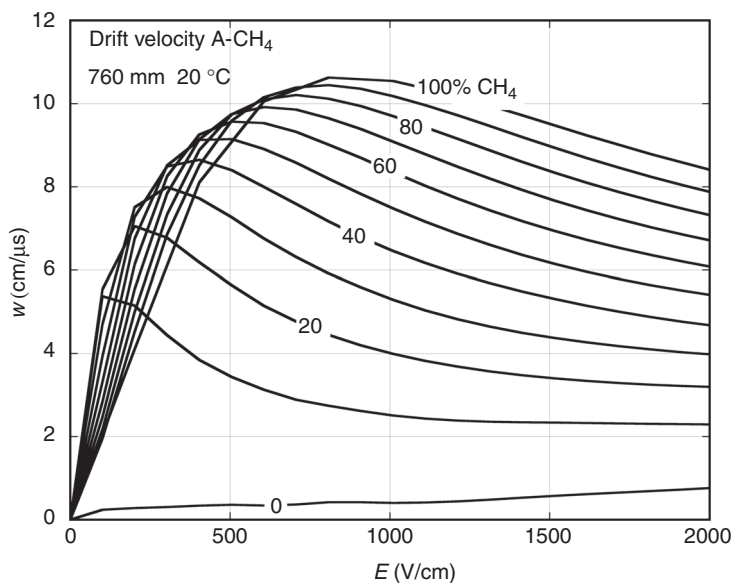


Figure 4.63 Computed drift velocity as a function of field for argon–methane mixtures at NTP.

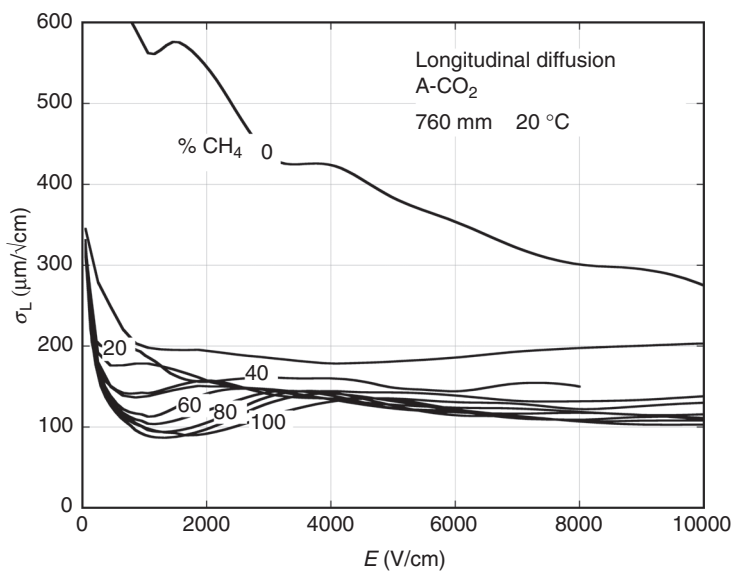


Figure 4.64 Standard deviation of the longitudinal diffusion for 1 cm drift, as a function of field, for argon–carbon dioxide mixtures at NTP.

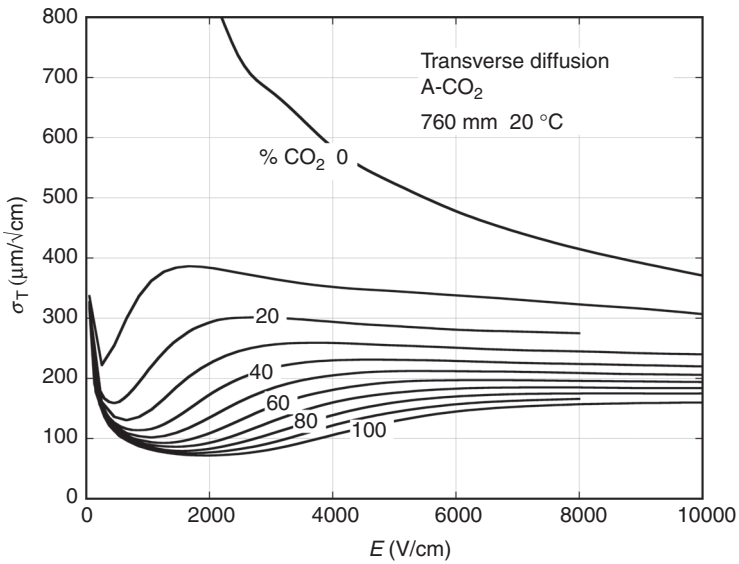


Figure 4.65 Transverse diffusion for 1 cm drift as a function of field for argon-carbon dioxide mixtures at NTP.

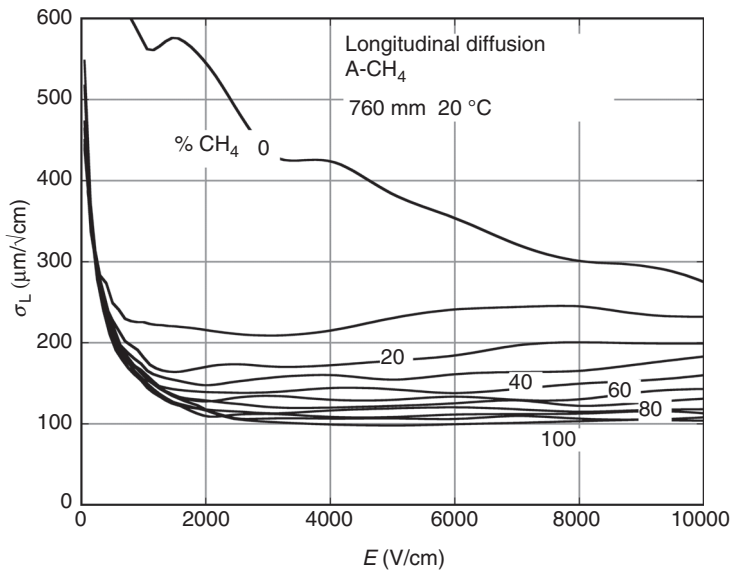


Figure 4.66 Longitudinal diffusion for 1 cm drift as a function of field for argon-methane mixtures at NTP.

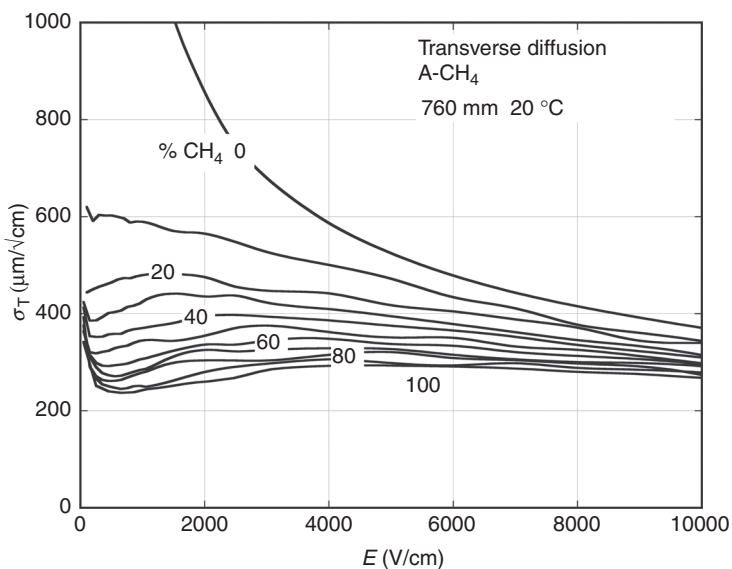


Figure 4.67 Transverse diffusion for 1 cm drift as a function of field for argon–methane mixtures at NTP.

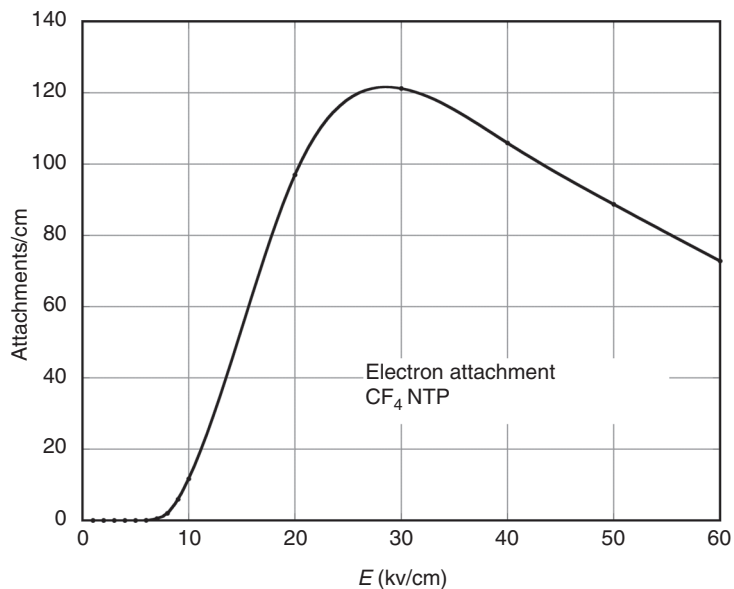


Figure 4.68 Electron attachments/cm of drift in carbon tetrafluoride as a function of field.

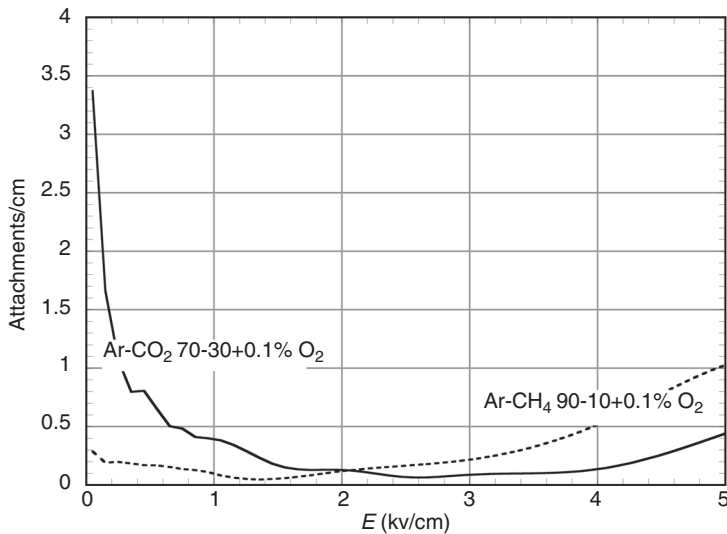


Figure 4.69 Electron attachments/cm as a function of field for equal addition of oxygen to argon–carbon dioxide and argon–methane mixtures.

Examples of drift velocity and diffusion for a range of gases and mixtures commonly used in detectors are given in Figure 4.59 to Figure 4.67; all data have been computed for gases at NTP with the program MAGBOLTZ.

The presence of an external magnetic field modifies the drift and diffusion properties of electrons, in particular reducing the transverse diffusion, as discussed in Section 4.6. This basic property, that permits one to largely improve the localization accuracy on long drift detectors, is exploited in time projection chambers; plots of drift and diffusion properties for several cases used in these devices are given in Section 10.5.

As it includes the attachment cross sections, the program allows also computation of the electron losses in pure gases and mixtures. Figure 4.68 provides the capture probability, expressed in attachments/cm, for pure carbon tetrafluoride at NTP, as a function of field: the large value at around 30 kV/cm reflects the corresponding peak in the cross section for electron energies approaching 10 eV (Figure 4.54). As at these high fields electrons already experience charge multiplication, losses are partly compensated by the increase of the overall charge. Experimental data on electron attachment in CF₄ are given in Anderson *et al.* (1992).

As another example Figure 4.69 shows the capture losses for equal additions of oxygen (0.1%) to argon–carbon dioxide and argon–methane; the very large difference in capture probability at low field in the first mixture is apparent, as already shown by the experimental results presented in Section 4.8.